Journal of Structural Geology 33 (2011) 399–421

Contents lists available at ScienceDirect

Journal of Structural Geology

journal homepage: www.elsevier.com/locate/jsg

# Deciphering cryptic P–T-d–t histories in the western Thor-Odin dome, Monashee Mountains, Canadian Cordillera: A key to unravelling pre-Cordilleran tectonic signatures

M. Iole Spalla [a,*], Davide Zanoni [b], Paul F. Williams [b], Guido Gosso [a]

[a] Dipartimento di Scienze della Terra "A. Desio", Università di Milano and CNR-IDPA, Via Mangiagalli, 34, 20133 Milano, Italy
[b] Department of Geology, University of New Brunswick, 2 Bailey Dr. Fredericton, NB, Canada E3B 5A3

ARTICLE INFO

*Article history:*
Received 3 May 2010
Received in revised form
16 November 2010
Accepted 17 November 2010
Available online 2 December 2010

*Keywords:*
P–T-d–t paths
HT exhumation
HT transposition
Tectonometamorphic memory

ABSTRACT

A detailed structural and metamorphic study along a transect from the core of the Thor-Odin dome to its western margin (South-eastern Canadian Cordillera) has allowed the reconstruction of the P–T-d–t history estimating PT changes, during successive fabric development. The dome comprises a recumbently-folded and transposed Proterozoic high-grade basement and Late Proterozoic-Palaeozoic metasedimentary cover, characterised by a regional foliation ($S_T$). An inferred, nearly-isothermal decompressional path, from a maximum depth of ca. 40 km, transgresses the "maximum relaxed geotherm", consistent with exhumation during lithospheric extension. Contrasting pre-$S_T$ PT conditions indicate that different units followed different PT paths before $S_T$ development. Traces of these early and variable structural and metamorphic re-equilibration steps are preserved in meter-scale boudins and granular-scale domains poorly affected by transposition. The various paths represent events, from Palaeoproterozoic to Proterozoic Rodinia break up, to Jurassic-Cretaceous convergence and final exhumation in the Eocene. Much of the deformational and metamorphic history may have been accumulated before onset of $S_T$. However, the early structural history is overprinted, and mineral assemblages and their relative ages are mostly obscured by $S_T$ development. A glimpse of the earlier geologic history is possible only by combining micro-structural analysis and PT estimates.



## 1. Introduction

P–T–t (Pressure, Temperature and relative or absolute time) and/or P–T-d–t (Pressure, Temperature and relative deformation time) paths integrated with thermal and mechanical models (e.g. Thompson, 1981; Cloos, 1993; Stöckhert and Gerya, 2005; Spalla and Marotta, 2007; and refs therein), produced to simulate the dynamics of convergent and divergent tectonic environments, have been widely used to elucidate the geodynamic evolution of orogenic domains (Spalla et al., 2010 and refs therein).

Reference to a previously defined structural history is essential for reconstruction of P–T-d–t paths (Spalla, 1993; Johnson and Vernon, 1995), due to the number of factors (rock type, P-T-fluid conditions, deformation history, diffusion etc…) influencing the accomplishment of metamorphic reactions during deformation (e.g. Williams, 1985; Vernon, 1989; Passchier and Trouw, 1996; Spalla et al., 2000; Brown, 2001; Hobbs et al., 2010). For this purpose, emphasis in the field has to be on establishing sequences of fabric overprinting and on distribution of fabric gradients (e.g. Williams, 1985). This involves sampling the widest range of thermo-mechanical stages and discrimination of micro-structural sites in which evidence of the metamorphic and deformational history is best preserved. Our sampling strategy therefore, is based on the assumption that rocks, which preserve a relatively longer metamorphic memory, are those in which the superposed planar fabrics are less evolved locally. Consequently, the structural correlation in a heterogeneously deformed area has to be grounded on geometrical criteria and metamorphic compatibility of the mineral assemblages defining the different fabrics.

Our aim is to produce an accurate reconstruction of the P–T-d–t evolution of rocks from the Thor-Odin dome (Fig. 1) in order to shed light on debated tectonic interpretations (e.g. Brown and Carr, 1990; Brown et al., 1992; Johnston et al., 2000; Kruse and Williams, 2007). For this purpose new results are presented for metapelites and amphibolite boudins sampled along a 5 km long E–W transect from the core of the dome to its western margin

* Corresponding author. Tel.: +39 (0)250315550; fax: +39 (0)250315494.
*E-mail addresses:* iole.spalla@unimi.it (M.I. Spalla), dzanoni@unb.ca (D. Zanoni), pfw@unb.ca (P.F. Williams), guido.gosso@unimi.it (G. Gosso).

0191-8141/$ – see front matter © 2010 Elsevier Ltd. All rights reserved.
doi:10.1016/j.jsg.2010.11.014

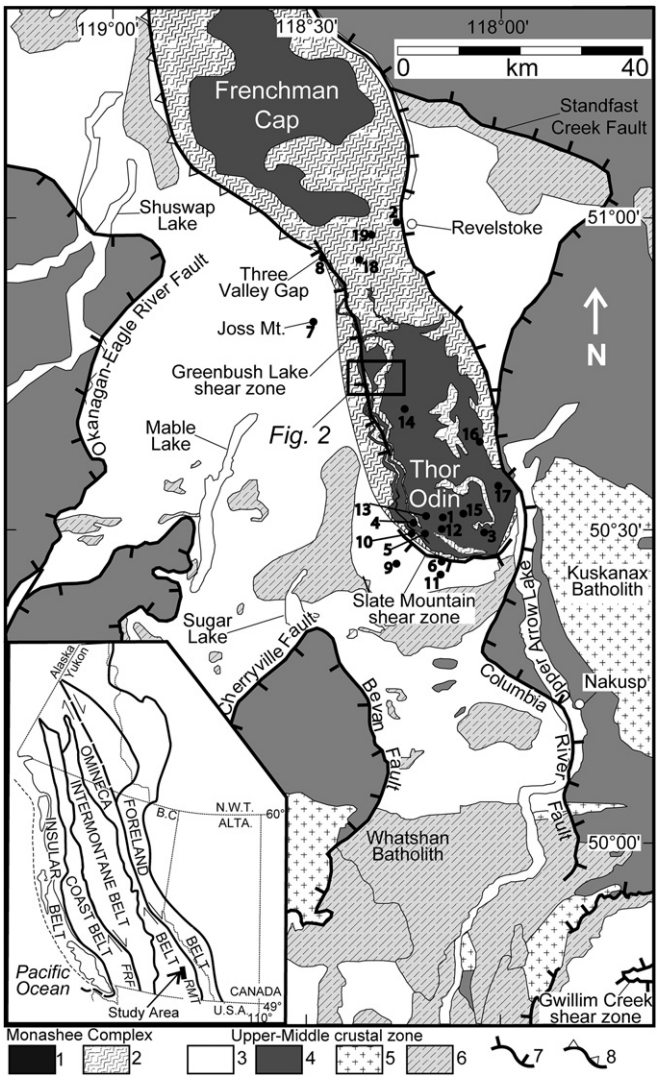


**Fig. 1.** Geological sketch map of the Omineca belt at the latitude of the Thor-Odin dome, modified after Carr (1991). 1 = Proterozoic North American basement rocks. 2 = Late Proterozoic or younger North American cover sequence. 3 = Late Proterozoic – Mesozoic metamorphic assemblages. 4 = Palaeozoic – Lower Jurassic stratified rocks. 5 = Jurassic plutonic rocks. 6 = Cretaceous – Eocene plutonic rocks. 7 = fault and shear zones; teeth are on the hanging wall. 8 = Monashee décollement; triangles on the hanging wall. Rectangle with the thick outline locates Fig. 2. Black dots and bold numbers locate the age data shown in Table 1a. Monashee décollement has been drawn only north of Three Valley Gap as shown by Read and Brown (1981), Journeay (1986) and Brown et al. (1992), we have found no evidence of its southward prolongation. Inset map shows the five belts constituting the Canadian Cordillera according to Gabrielse et al. (1991); RMT = Rocky Mountain Trench; FRF = Fraser River Fault.

(Greenbush Lake shear-band zone = GLSBZ; Figs. 1 and 2). The deformation history has been determined by means of detailed mapping (Kruse et al., 2004) and structural analysis (Johnston et al., 2000; Williams and Jiang, 2005; Kruse and Williams, 2007). The sequence of metamorphic reactions has been inferred taking into account the timing of mineral growth with respect to successive stages of fabric development. Subsequently PT conditions have been derived from chemical data acquired for minerals defining chronologically-selected fabric elements.

Using fabric evolution and the sequence of mineral assemblages supporting the fabrics in various rock groups, together with numerous radiometric data available in the literature (Table 1a and 1b and Fig. 2), we construct a relative chronology of tectonometamorphic stages.

Mineral abbreviations are as in Kretz (1983) after Whitney and Evans (2010) except for white mica (Wm).

## 2. Geological setting

The Canadian Cordillera comprises five belts, parallel to the strike of the chain, that differ in lithostratigraphic associations, and tectonic style *viz.* the Foreland, Omineca, Intermontane, Coastal and Insular belts (inset of Fig. 1). Major tectonic boundaries commonly separate these belts. The Omineca belt represents the hinterland of the Foreland belt and was exhumed as a result of the collision between the accreted terranes (Intermontane, Coastal and Insular belts) and the North American (Laurentian) margin (Monger et al., 1982; Gabrielse et al., 1991) between Middle-Late Jurassic and Cretaceous (Gibson et al., 2008).

The Monashee complex is one of the structural culminations of the southern Omineca belt, which exposes the deepest part of the Canadian Cordillera. It is divided into two domes: Frenchman Cap and Thor-Odin (Fig. 1). The cores of these domes consist of Palaeoproterozoic basement with high-grade polymetamorphic migmatitic para- and ortho-gneisses and metabasics as well as Proterozoic intrusions (Reesor and Moore, 1971; Wanless and Reesor, 1975; Armstrong et al., 1991; Parkinson, 1991; Carr, 1995; Crowley, 1997). This basement is overlain unconformably (Ross and Parrish, 1991 and refs. therein) by a Proterozoic to Palaeozoic metasedimentary sequence, comprising quartzites, pelitic schists, semi-pelitic schists, marbles, calcsilicate gneisses, and various quartzo-feldspathic gneisses (e.g. Brown, 1980; Kruse et al., 2004). At all scales from regional to microscopic, basement to cover are repeated by transposition, and the ratio of cover and basement increases upwards.

The Monashee complex is tectonically overlain by relatively lower grade (amphibolite and greenschist facies) metamorphic rocks, which comprise a unit known in the literature as the Selkirk Allochthon (Brown et al., 1992). The boundary between Monashee complex and the Selkirk Allochthon, in the Thor-Odin dome, like all boundaries in the complex, is strongly transposed by folding into a common $S_T$ (Johnston et al., 2000; Kruse et al., 2004; Kruse and Williams, 2007).

The ubiquitous transposition fabric ($S_T$) is the product of a penetrative non-coaxial flow. The sense of shear is consistently top-to-the-northeast in the Monashee complex and the lower part of the Selkirk Allochthon, and is top-to-the-southwest at higher structural levels (Journeay, 1986; Johnston et al., 2000; Williams and Jiang, 2005; Kuiper et al., 2006). The western boundary of the Thor-Odin dome is marked by a west dipping high strain zone with a top-to-the-west sense of shear, successively overprinted by north–south trending Eocene brittle strike-slip, and normal, faults (Johnston et al., 2000; Kruse and Williams, 2007). Spatially, the normal shear zone coincides approximately with the southern prolongation of the Monashee décollement and the transition between the Monashee complex and the Selkirk Allochthon (Journeay and Brown, 1986; Brown et al., 1992; McNicoll and Brown, 1995). The Monashee décollement is an interpreted top-to-the-northeast movement zone for which no evidence is found, along the transect here discussed, other than the ubiquitous transposition foliation (Johnston et al., 2000; Spark, 2001; Kruse and Williams, 2007).

The Monashee complex is characterised by amphibolite to granulite facies conditions, a significantly higher metamorphic grade than is found in surrounding areas (Journeay, 1986; Johnston et al., 2000). In Fig. 3, PT estimates for dominant metamorphic imprints in the northern (Ghent et al., 1977; Lane et al., 1989; Nyman et al., 1995) and southern (Norlander et al., 2002) Thor-Odin dome are summarised with details of whole rock composition and sample locations. Earlier estimates plot between amphibolite

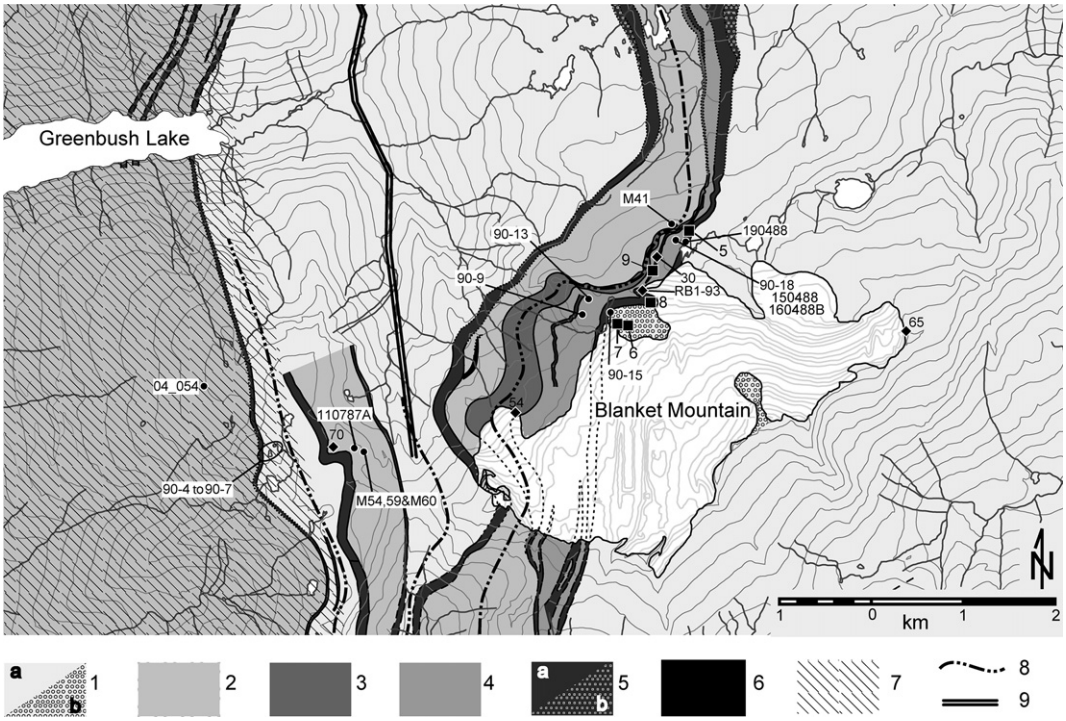


**Fig. 2.** Geological map of the area between Blanket Mt. and GLSBZ, modified after Kruse et al. (2004). *Basement sequence (Proterozoic)*: 1a) Undifferentiated para- and ortho-gneisses dominated by Bt–Fsp–Qz-migmatitic gneisses, with metabasic boudins or layers; 1b) Hbl-Bt granodioritic gneisses, with metabasic boudins. *Intermingled cover and basement rocks*: 2 = Undifferentiated paragneisses with pelitic schists, calc-silicate gneisses, metabasics and minor marbles. *Metasedimentary cover sequence (Proterozoic to Palaeozoic?)*: 3 = pelitic and semi-pelitic schists and gneisses, commonly containing Bt, Grt, and Sil; 4 = calc-silicate gneiss containing Cpx, Pl, Tr and Qz; 5 = quartzite (a) and quartzitic gneisses (b) with Sil, Kfs, Bt, Wm, and Tur; 6 = marbles. 7 = Greenbush Lake shear-band zone. *Symbols*: 8 = Axial surface trace of $F_2$ folds; 9 = Victor Creek fault. Black dots locate the samples with the most significant microstructural features and those analysed using the microprobe. Black diamonds locate U–Pb Zrn and Mnz radiometric ages after Kuiper (2003); black squares locate U–Pb Zrn and Mnz radiometric ages after Johnston et al. (2000); labels refer to dated specimens listed in Table 1b.

and Sil-granulite facies; the more recent fall between Ky-granulite and Sil-granulite facies, according to Ernst and Liou (2008): this misfit can depend on the refinement of the thermobarometers. Only the thermal-peak conditions have been estimated and no quantitative P–T–t or P–T-d–t paths are inferred by the cited authors (Fig. 3). Norlander et al. (2002) suggest that Thor-Odin was exhumed by isothermal decompression involving the partial melting of a thickened continental crust (ca. 60 Ma), with melt accumulation in the mid-lower crust. The melt-weakened rock rose diapirically (ca. 56 Ma), and tectonic unroofing was accommodated by shallow-dipping normal faults.

Igneous and metamorphic ages for the Thor-Odin dome range from Late Archean to Tertiary; details of location, rock type, method, error and age significance are shown in Table 1a for the Thor-Odin dome (Fig. 1) and Table 1b for the Blanket area (Fig. 2). The oldest ages (Table 1a), ranging from 1610 ± 120 and 2730 ± 210 Ma are interpreted as ages of igneous protoliths (Duncan, 1982; Armstrong et al., 1991; Parkinson, 1992; Kuiper, 2003; Vanderhaeghe et al., 1999). Other igneous ages or ages of migmatisation range from Middle to Late Proterozoic (Table 1a; Duncan, 1982, 1984). Alternatively they may be interpreted as mixed ages. Ages for detrital Zrn from quartzites, of approximately 1770 ± 1.1 Ma (Coleman, 1990) and 1825 ± 6 Ma (Kuiper, 2003) have recently been superceded by ages of 566.7 ± 11.0 Ma (Shields and Kuiper, 2008) and 608 ± 35 Ma (youngest concordant analysis; van Rooyen et al., 2010) from Blanket Mt. and Mount Symonds respectively. This confirms that at least these cover quartzites are of Palaeozoic age.

Except for an old metamorphic age of 175 Ma (+146 − 162 Ma; 2$\sigma$ error), determined from a lower intercept of a discordant multi-grain Zrn fraction from a foliated metagranodiorite from the southeast of the complex (Wanless and Reesor, 1975), the most important cluster of metamorphic ages in the Thor-Odin dome, is for metapelites, metagranitoids, and metabasics (see Table 1 for details), ranging from 60 to 51 Ma (Parrish et al., 1988; Coleman, 1990; Carr, 1995; Johnston et al., 2000; Kuiper, 2003; Vanderhaeghe et al., 1999; Hinchey, 2005; Hinchey et al., 2006). Older metamorphic ages are recorded west of GLSBZ in the Selkirk Allochthon (ca. 93.0 ± 1.5 Ma; Johnston et al., 2000) and in amphibolite boudins from the Thor-Odin dome (ca. 73 Ma; Parkinson, 1992), close to the top-to-the-west shear zone at the boundary with the Selkirk Allochthon (Fig. 1 and Table 1).

Anatectic leucosomes, in the southwest of the complex, crystallised between 56 and 52 Ma (Hinchey et al., 2006). Ky-bearing pegmatites, in boudin necks in the cover sequence of Blanket Mt., are dated at 54.5 ± 1 Ma. They are followed by 52–50 Ma pegmatites, which intersect $F_3$ folds (Johnston et al., 2000; see Table 1b), and by lamprophyre dykes dated at 50–48 Ma (Adams et al., 2005; Table 1a). Fission track data indicate cooling at $T$ below 120 and 250 °C between 40 and 44 Ma (Lorencak et al., 2001; Table 1a).

## 3. Deformation history

A sequence of structures related to successive deformation stages, according to their kinematic compatibility and geometrical affinities, is described for the study area (Fig. 2). It is summarised in detail in Table 2 and described below, together with age data and relationships to successive emplacements of melt.

### 3.1. $D_T$

Regionally, the transposition foliation $S_T$ (Fig. 4a) (Williams and Jiang, 2005) is interpreted as having developed by repeated

**Table 1a**
Review of radiometric ages in Thor-Odin dome. Labels locate samples in Fig. 1.

| Label on Fig. 1 | Locality | Rock | Mat. | Method | Age (Ma) | Notes | Author |
|---|---|---|---|---|---|---|---|
| 1 | Mt. Thor-Mt. Odin area | Migmatized granite | Zrn | U/Pb | 2000 ± 400<br>2000 ± 200 | Inheritance | Vanderhaeghe et al., 1999, 2003 |
| | | Orthogneiss | Zrn | U/Pb | 1874 ± 21<br>1934 ± 6 | Igneous crystallisation | Parkinson, 1991 |
| | | Migmatitic metagranitoid | WR | Rb/Sr | 860–750 | Migmatisation | Duncan, 1982, 1984 |
| | | Metagranitoid | Zrn | U/Pb | 175 + 146–162 | Metamorphic | Wanless and Reesor, 1975 |
| | | Migmatite | Zrn | U/Pb | 54.6 ± 1.4<br>55.9 ± 3.1 | Anatectic melt crystallization | Vanderhaeghe et al., 1999 |
| | | – | Zrn | FT | 52.9 ± 5.4 | Cooling | Lorencak et al., 2001 |
| | | | Ap | | 43.7 ± 4.0 | | |
| 2 | Mt. English area | Leucogneiss | WR | Rb/Sr | 1610 ± 120 | Igneous crystallisation | Armstrong et al., 1991 |
| | | Metadiorite | | | 2462 ± 1470 | | |
| 3 | SE part of the dome | Bt–Qz–Fsp gneiss | Zrn | U/Pb | 2061 ± 99 | Inheritance | Parkinson, 1991 |
| 4 | Mt. Gunnarson | Core gneiss, unmigmatized | WR | Rb/Sr | 2730 ± 210 | Igneous crystallisation | Duncan, 1982 |
| 5 | Icebound Lake area | Quartzite | Zrn | U/Pb | 1771.5 ± 1.0<br>1749.7 ± 1.1<br>1768.3 ± 1.2 | Detrital | Coleman, 1990 |
| | | Paragneiss | Mnz | TIMS | 60.6 ± 0.4 | Metamorphic peak | |
| | | Pegmatite | | | 54.0 ± 1.5 | | |
| 6 | Mt. Symonds area | Quartzite | Zrn | U/Pb | 608 ± 35 | Detrital | van Rooyen et al., 2010 |
| | | Amphibolite | | | 61.0 ± 0.5 | Metamorphic | Carr, 1995 |
| 7 | Joss Mountain | Schist | Zrn | U/Pb | 93.0 ± 1.5 | Metamorphic peak | Johnston et al., 2000 |
| | | Orthogneiss | | | 362 ± 13 | Protolith | Kuiper, 2003 |
| | | Pegmatite | Mnz | U/Pb | 69.6 ± 2.5 | Crystallisation | |
| | | Pegmatite | | | 55.4 ± 0.6 | Late alteration | |
| 8 | Three Valley Gap and Victor Lake | Grt-amphibolite | Zrn | U/Pb | 73.0 ± 1.7 | Metamorphic peak | Parkinson, 1992 |
| | | Paragneiss | Mnz | | 71.7 ± 1.5 | Metamorphic | Kuiper, 2003 |
| | | – | Zrn | FT | 49.2 ± 4.0 | Cooling | Lorencak et al., 2001 |
| | | | Ap | | 30.2 ± 2.8 | | |
| | | | Zrn | | 49.0 ± 4.4 | | |
| | | | Ap | | 43.3 ± 4.2 | | |
| 9 | Mount Fosthall area | Amphibolite | Spn | U/Pb | 55.0 ± 1.0 | Metamorphic | Carr, 1995 |
| | | | Spn,Zrn | U/Pb | 60.0 ± 1.0 | | |
| 10 | Cariboo Alp | Amphibolite | Spn | U/Pb | 58.0 ± 4.0 | Metamorphic | Carr, 1995 |
| 11 | Fosthall Creek | Mylonitic granite | Fsp, Ms | Rb/Sr | 53.9 ± 0.8<br>56.0 ± 0.9 | Metamorphic | Parrish et al., 1988 |
| 12 | Bearpaw Lake | Grt–Crd–Ged-boudin | Mnz | U/Pb | 56.2 ± 1.2<br>54.27 ± 1.0 | Metamorphic peak | Hinchey, 2005 |
| | | Quartzite | | | 52.5 ± 0.8 | Isothermal decompression | |
| 13 | Saturday Glacier | Folded leucosome | Zrn | U/Pb | 55.5 ± 0.6<br>54.2 ± 0.8 | Anatectic melt crystallization | Hinchey et al., 2006 |
| | | Pegmatitic leucosome | | | 52.5 ± 1.0<br>54.7 ± 4.0 | | |
| | | Leucosome | | | 2564 ± 6<br>1856 ± 12 | Detrital | |
| 14 | Cranberry Valley | Crosscutting aplite | Mnz | U/Pb | 52.3 ± 3.0 | Crystallisation | Kuiper, 2003 |
| | | | Zrn | U/Pb | 52.7 ± 0.6 | | |
| | | | | | 1952 ± 4<br>2087 ± 2 | Possibly inheritance | |
| | | Folded pegmatite | Zrn | U/Pb | 1949 ± 2<br>2013 ± 2 | | |
| | | | Mnz | U/Pb | 51.0 ± 1.0 | Crystallisation | |
| | | | Zrn | | 51.8 ± 0.7 | | |
| 15 | Frigg Glacier | Crosscutting aplite | Zrn | U/Pb | 1792 ± 49 | Crystallisation or inheritance | Kuiper, 2003 |
| | | | | | 47.9 ± 11.0 | Crystallisation or later event | |
| 16 | E of Mount Hall | – | Zrn | FT | 37.5 ± 5.0<br>43.0 ± 4.2 | Cooling | Lorencak et al., 2001 |
| | | | Ap | | 28.8 ± 4.4 | | |
| 17 | Pingston Creek | – | Zrn | FT | 53.9 ± 5.6 | Cooling | Lorencak et al., 2001 |
| | | | Ap | | 39.5 ± 3.2 | | |
| 18 | N of Mount McPherson | – | Zrn | FT | 44.2 ± 7.6 | Cooling | Lorencak et al., 2001 |
| | | | Ap | | 40.1 ± 5.0 | | |
| 19 | W of Revelstoke | – | Ap | FT | 27.7 ± 3.4 | Cooling | Lorencak et al., 2001 |
| Various locations | Northern part of the dome | Lamprophyre | Bt | Ar/Ar | 51.0–55.0 | Crystallisation | Adams et al., 2005 |
| | | Country rock | Wm | Ar/Ar | 48.4 ± 0.3 | Contact metamorphis | |

**Table 1b**
Review of radiometric ages along Blanket-GLSBZ transect. Labels locate samples in Fig. 2.

| Label on Fig. 2 | Rock | Mineral | Method | Age (Ma) | Notes | Author |
|---|---|---|---|---|---|---|
| 5 | Cover Sil schist | Mnz | U/Pb | 57.1 ± 0.6 | | Johnston et al., 2000 |
| 6 | Basement Sil schist | Mnz | U/Pb | 55.5 ± 0.5 | | |
| 7 | Pegmatite (relic Ky) | Mnz | U/Pb | 54.5 ± 1.0 | In a neck of $F_1/F_2$ in the cover | |
| 8 | Pegamatite | Zrn & Mnz | U/Pb | 51.5 ± 0.5 | Cuts $S_2$ and $F_3$ folds | |
| 9 | Tur-pegamatite | Mnz | U/Pb | 50.2 ± 0.5 | | |
| 30 | Quartzite | Mnz | U/Pb | 54.2 ± 0.3 | Metamorphic | Kuiper, 2003 |
| | | Zrn | U/Pb | 1825 ± 6.0 | Detrital Zrc | Shields and Kuiper, 2008 |
| | | | | ~560 | | |
| 54 | Cover schist | Mnz | U/Pb | 54.5 ± 1.2 | Metamorphic | Kuiper, 2003 |
| | | Zrn | U/Pb | 52.6 ± 6.3 | | |
| 65 | Migmatitic basement orthogneiss | Zrn | U/Pb | 2100 ± 21 | Protolith age | Kuiper, 2003 |
| | | | | 1811 ± 14 | Possible migmatisation | |
| | | | | 52.0 ± 2.0 | Metamorphic age or rejuvenated by fluids | |
| | | Mnz | U/Pb | 51.6 ± 0.7 | Later recrystallisation | |
| 70 | Cover schist | Mnz | U/Pb | 60.7 ± 12.5 | Metamorphic | Kuiper, 2003 |

folding in a non-coaxially flowing infrastructure zone. Tightening of the folds until isoclinal and generally rootless, resulted in the development and repeated modification of $S_T$. At least three generations of folds can be recognised, but they are generally divided into mature and immature types (Table 2). Mature folds may be referred to as $F_1$ or $F_2$ (Fig. 4b), depending on local overprinting relationships, but no regional significance is attributed to this classification, whilst immature folds may be referred to as $F_3$ (Table 2 and Fig. 4c). Whatever their origin, the ultimate fate of all folds involved in the transposition is to become mature recumbent isoclines with axial surfaces parallel to $S_T$, and hinge-lines generally parallel to the transport direction. Since $F_1$–$F_3$ folds in their present form, are, at least in part, a product of the non-coaxial-flow-related transposition (Williams and Jiang, 2005), we refer to them collectively as $D_T$ structures, whilst recognising that they may have developed during earlier deformation and be simply modified by $D_T$.

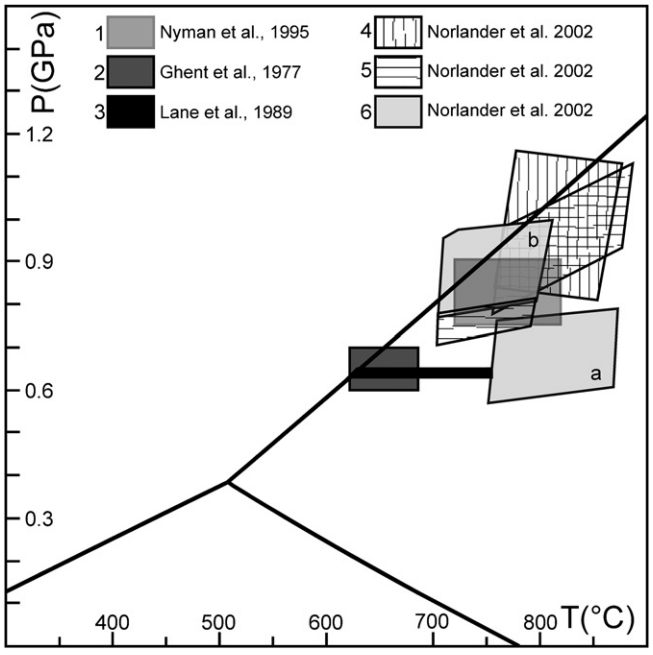


**Fig. 3.** Summary of PT estimates for the Thor-Odin dome from the literature. Legend: 1 = Sil-bearing migmatites from Three Valley Gap after Nyman et al. (1995); 2 = Cpx–Grt-bearing amphibolites from Three Valley Gap after Ghent et al. (1977); 3 = metapelites from Revelstoke after Lane et al. (1989); samples from Bearpaw Lake and Saturday Peak after Norlander et al. (2002): 4 = Ged-Crd rocks, 5 = metapelitic rocks, 6a = Grt–Amp-bearing rocks, Ti-oxide-free, and 6b = Grt–Amp-bearing rocks with Ti-oxides.

Locally there are faults that have ramp/flat geometry such that they ramp across $S_T$ and deflect at either end into parallelism with $S_T$. They are identified by the ramps and the abrupt change in local lithostratigraphy (Table 2) and are interpreted as normal faults. This is consistent with spatially related minor structures, and it is believed that they are a mechanism for thinning perpendicular to $S_T$ (Jiang and Williams, 1998) during final stage of transposition. An example of such a structure is shown in Fig. 4a, where rocks of both the footwall and hanging wall are cut by generally undeformed Tur-pegmatite dykes that are perpendicular to $S_T$ indicating that there was no penetrative deformation in the country rock during the final stages of $S_T$.

We interpret these data (Table 2) as follows: the fault developed late during $D_T$ deformation, after local cessation of transposition, by $S_T$-parallel shear and local ramping across $S_T$. The fault and $S_T$ were subsequently folded by a regional-scale transposition-related dragfold, which developed late enough to be preserved as an immature fold ($F_3$). Pegmatite intruded into the ramp during faulting and locally dates the end of $S_T$ development. Since cover and basement are transposed together the transposition must be post late Neoproterozoic (see Table 1). In the studied transect $F_3$ predates 50.2 ± 0.5 Ma pegmatite (Tables 1b and 2; Johnston et al., 2000) and a ca. 54 Ma Sil-after-Ky-bearing pegmatite occurs in an $S_T$-related boudin neck (Johnston et al., 2000) indicating that $S_T$ development was underway at least during the time bracketed by these two dates (Table 2).

### 3.2. $D_{T+1}$

Upright dome-wide folding is largely responsible for the Thor-Odin culmination, even though definitive outcrop-scale evidence of these folds is rare in many parts of the dome. They are referred to as $F_4$ or $D_{T+1}$ structures (Table 2). $F_4$ occurs as parasitic folds throughout the dome (Fig. 4d), except on the steep west limb of the regional structure. Overprinting relationships between $F_3$ folds and $D_{T+1}$ structures are rare, but $D_{T+1}$ is consistently younger. In addition, the gradual morphological transition between $F_1$ and $F_3$ folds supports their interpretation as products of a continuous flow. Whereas the different morphology of $F_4$ folds indicates, that they belong to a different flow regime, $D_{T+1}$.

Throughout Thor-Odin there is evidence of late $S_T$-parallel syn-$D_{T+1}$ shear (Table 2). On the west limb of the culmination, since the sense of shear is the same as for $D_T$, the shear zones are only distinguishable from $S_T$-related shear, where they cut post-$S_T$ pegmatites (Fig. 4e). The regional distribution of the shear zones

**Table 2**
Summary of the main structural features characterising the deformation stages $D_T$, $D_{T+1}$ and $D_{T+2}$ and their relationships with absolute ages.

| Stage | Mesostructure type | Mesostructure style | Kinematics | Melt emplacement | Ages |
|---|---|---|---|---|---|
| $D_T$ | Transposition foliation ($S_T$) | Composite transposition foliation ($S_T$) largely defined by compositional domains and generally associated with a shape foliation (S foliation of Berthé et al., 1979), which is inclined to $S_T$ at angles of $\sim 30^\circ$ or less and is everywhere anticlockwise of $S_T$ looking northwest. Regionally $S_T$ is approximately horizontal (Fig. 4a). | Top-to-the-NE non-coaxial flow | Ky-bearing pegmatite in a boudin neck in syn-$S_T$ boudin (Johnston et al., 2000). | Younger than early Palaeozoic quartzite of cover (Shields and Kuiper, 2008); active at 54 Ma (Ky-bearing pegmatite age; Johnston et al., 2000). |
| | Mature folds ($F_1$, $F_2$) | Tight to isoclinal folds (Fig. 4b); transpose earlier markers into $S_T$. Axial surfaces are parallel or nearly parallel to $S_T$. Some $F_1/F_2$ folds developed as dragfolds in $S_T$ (Lister and Williams, 1983; Williams and Jiang, 2005). | Top-to-the-NE non-coaxial flow; hinges show evidence of rotation towards the NE-transport direction. | | |
| | $F_3$ immature folds | More open than $F_1$ and $F_2$ folds (Fig. 4c); axial planes inclined to $S_T$; hinges generally close to perpendicular to the transport direction. $F_3$ folds are dragfolds perturbing $S_T$. | Top-to-the-NE non-coaxial flow. | | Predate 50.2 ± 0.5 Ma (pegmatites age; Johnston et al., 2000). |
| | $S_T$–related ramp/flat faults | Ramps dip easterly. | Easterly-verging low angle normal fault. | Boudin necks injected by Tur-pegmatite. | 50.2 ± 0.5 Ma (pegmatites age; Johnston et al., 2000). |
| $D_{T+1}$ | Open upright folds parasitic on asymmetrical regional $F_4$ pericline | Steep W-dipping west limb and shallow E-dipping east limb. Northerly trending axial plane, variable plunge. In the Blanket area there are open $F_4$ folds in the eastern portion of the transect and immediately west of the Victor Creek fault. | | | |
| | Narrow $S_T$–parallel shear zones on limbs of upright flexural slip folds | Top-to-the-E shear zone cuts Tur-pegmatite reducing it to a string of boudins locally (Fig. 4e). | Flexural-slip-related top-to-the-NE (W limb) and top-to-the-SW shear (E limb) on alternate limbs of $F_4$ folds. | | Shear zone overprints Tur-pegmatite (Fig. 4e) dated at 50.2 ± 0.5 Ma (Johnston et al., 2000) and is syn $F_4$ folding which is older than lamprophyres which have ages close to 50–48 Ma (Adams et al., 2005). |
| | | | | Late grey granitic melt | It overprints $F_3$ folds, and is deformed by $F_4$-related shear. Overprints most pegmatites and aplites, but is overprinted by at least one aplite. Interpreted as syn-$D_{T+1}$ folding. |
| $D_{T+2}$ | Normal shear zones reactivating $S_T$, cut by shear bands; westerly plunge reactivated Sil lineation. | | Shear bands (Johnston, 1998), displaced veins and W vergent folds indicate top-down-to-the-west shear. Displaced markers also indicate dextral transcurrent shear. | | |
| | Brittle faults striking parallel to the shear zone Slickenside striae | | Continuation of the dextral transcurrent, and down-to-the-west normal movement. Normal faults consistently overprint transcurrent faults. | | The lamprophyres overprint and are overprinted by the late faults indicating that they are coeval. |

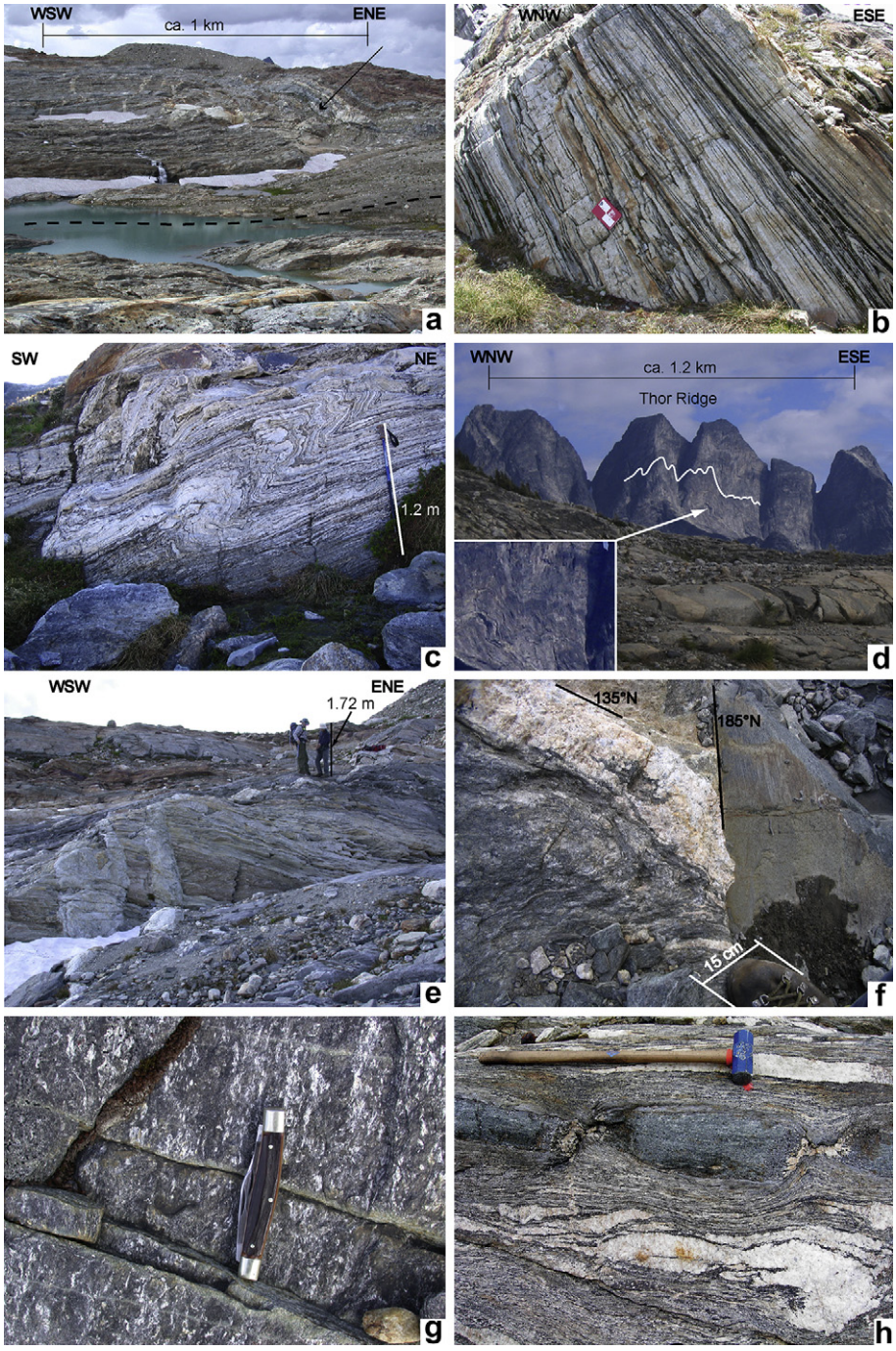


**Fig. 4.** a) $S_T$ in outcrop immediately N of Blanket Glacier; the dashed black line marks the contact between quartzites (above) and basement rocks (below). Arrow indicates the ramp. b) Intrafolial mature folds in calcsilicate within the GLSBZ on the plateau south of Greenbush Lake; long side of the field-book for scale = 20 cm. c) Immature fold affecting the $S_T$ in basement rocks from the southern slope of Blanket Mt. d) $D_{T+1}$ upright folds on the south face of Mount Thor; the white line traces one folded surface. The insect shows the $D_{T+1}$ parasitic folds in more detail without the white line. e) 50 Ma old pegmatite displaced by a dextral top to the NE shear zone in pelitic and semi-pelitic gneisses, plus minor quartzite, of the metasedimentary cover close to the northern margin of Blanket Glacier. f) Lamprophyre intersecting a ca. 50 Ma old pegmatite hosted by pelitic and semi-pelitic gneisses of the metasedimentary cover sequence close to the northern margin of Blanket Glacier. Strike of both dykes is indicated. g) West-plunging Sil-bearing lineation on $S_T$ in Ky-bearing metapelites close to the Victor Creek fault. Knife for scale 15 cm. h) Amphibolite boudins wrapped by Sil-bearing $S_T$, north of Blanket Glacier. Sledge hammer handle for scale ca. 90 cm.

with opposite senses of shear on the opposite limbs of the regional fold is consistent with flexural slip during $F_4$ folding, so they are interpreted as $D_{T+1}$ structures (Table 2).

Lamprophyre dykes in the Blanket area are undeformed by $D_{T+1}$ structures and, as elsewhere in Thor-Odin, are steeply dipping irrespective of the orientation of $S_T$, i.e. irrespective of their position relative to $D_{T+1}$ folds. They generally cut pegmatitic and aplitic veins (Fig. 4f) and also cut a $D_{T+1}$ shear zone. The dykes are therefore interpreted as post $D_{T+1}$ (Table 2).

A fine-grained grey granitoid (late granitic melt, Table 2) occurs as irregular bodies and dykes, which contain decimetre sized xenoliths, matching country rocks in the immediate vicinity. Contacts between the veins and the country rock may be sharp or diffuse suggesting a local sourcing of the melt. The grey granitoid

overprints $F_3$ folds and intersects (with only one exception known to the writers) all pegmatites and aplites indicating that it postdates $D_T$ (Table 2 for details). It is deformed by $D_{T+1}$-related shear zones and strain localisation occurs where the shear zone pass from the country rock into the granitoid; on these grounds we tentatively interpret the granitoid as syn-$D_{T+1}$.

### 3.3. $D_{T+2}$

The limbs of the Thor-Odin $F_4$ pericline were reactivated as E- and W-dipping normal shear zones by the Columbia River Fault zone and GLSBZ respectively, further accentuating the domal appearance of the structure and making it a horst, as well as an antiform. Both zones also have dextral transcurrent components (Table 2). In the Blanket area, the shear zone deformation occurred by reactivation of $S_T$ (Johnston et al., 2000), and was associated with rotation and accentuation of the earlier Sil after Ky lineation (Fig. 4g). Where the shear zone lineation is well developed, there are microfractures approximately perpendicular to the lineation. The fractures are filled with retrograde minerals (Johnston, 1998; Kruse, 2007) signifying retrogression during $D_{T+2}$. Brittle structures suggest a continuation of the same kinematics with normal movement continuing longer than transcurrent movement (Table 2). These brittle structures are both the same age as, and younger than, the ca. 50–48 Ma old lamprophyres (see details in Table 2).

## 4. Microstructure

Samples related to the sequence of mesostructural events come from the northern slope of Blanket Mt., further west towards the Victor Creek fault, and from the GLSBZ bounding the dome to the west (Fig. 2). In this area, basement and cover rocks are repeatedly folded together, and foliated quartzites, marbles and calcsilicates inter-layered with foliated metapelites, contain layers or boudins of metabasics (Fig. 4h), which may be foliated or massive. The metapelites and metabasics are subdivided on the basis of mineral associations.

Micro-structural analysis is concentrated on the recognition of mineral assemblages representing successive stages of fabric evolution. This enables interpretation of the succession of crustal PT environments experienced by the Monashee complex during deformation (*viz* P–T-d–t path reconstruction). In addition, evaluation of the degree of re-crystallisation helps in locating microstructural sites for investigation of mineral compositional variation, the basis of accurate thermobarometry.

Sequential growth of the same mineral phases is indicated by addition of a Roman numeral to the mineral abbreviation.

### 4.1. Metapelites

In these rocks the transposition foliation $S_T$, is marked by the shape and lattice preferred Orientation (SPO and LPO) of BtII and Sil, which are concentrated in thin layers alternating with Qz–Fsp-layers. Ky porphyroclasts occur immediately east of the GLSBZ and Spl grains occur in the eastern margin of the zone, both as relics in $S_T$. Therefore, Ky-bearing, Spl-bearing, and Ky-Spl-free metapelites are described separately.

#### 4.1.1. Ky-bearing metapelites

The Ky porphyroclasts (Fig. 5a–c) define an SPO foliation parallel to $S_T$ and contain an internal foliation (Si), which is generally inclined at a high angle to Se = $S_T$. Si is defined by Qz, Fsp, Rt and locally BtI (Fig. 5b). Ky also encloses rare grains of Wm (Fig. 5c) and St. Grt porphyroblasts are wrapped by $S_T$, contain Qz, BtI, rare St and Rt rimmed by Ilm, and have strain shadows filled by Qz and Kfs. The inclusion grain-size is generally finer than that of the matrix and inclusions preferentially cluster in crystal cores (GrtI), leaving the rims mostly inclusion-free (GrtII) (Fig. 5a). Locally they are in trails at a high angle and/or asymptotic to Se. GrtII also forms trails of small grains in $S_T$ films, shows rational boundaries with the BtII grains marking $S_T$, and includes rare Bt and Qz. These microstructural features suggest a pre- to syn-$S_T$ Grt growth. BtI porphyroclasts are inclined to and wrapped by $S_T$. Sil generally forms in the strain shadows of Ky, and fibrolite partially replaces both prismatic Sil and Ky porphyroclasts at their rims. The Fsp-rich layers consist of Qz, Pl (PlI) and Kfs plus minor coarse-grained Bt crystals that show a weak SPO, parallel to $S_T$; PlI may contain small grains of Ky.

Reaction rims containing BtIII, Qz, PlII and rare Kfs occur between GrtII and BtII: where Grt forms $S_T$-parallel tails.

Kfs is locally interstitial to rounded PlI and Qz grains (Fig. 5d) and forms monocrystalline films along Ky fractures and cleavages, which contain rounded Qtz and Fsp. Ab may be interstitial to Kfs and PlI or forms a double monocrystalline film with Kfs between Qz and PlI. Similar microstructures have been interpreted as the effect of late, in situ, partial melting, occurring under very low-*P* conditions (e.g. Rosenberg and Riller, 2000; Holness and Sawyer, 2008).

Late fractures are generally filled by greenschist facies minerals: in Grt by Chl and rare Ab; in Sil (Fig. 5e) by Chl, Wm and locally by BtIV, widely replaced by Chl. Mostly, Wm and Chl filling the Sil fractures show an SPO perpendicular to the fracture walls. Chl, sagenitic Rt, and late Kfs replace Bt.

#### 4.1.2. Spl-bearing metapelites

$S_T$ in these metapelites is marked by LPO and SPO of BtII and Sil, and by layers of coarse-grained Kfs, Qz and Pl. Grt occurs as porphyroblasts, which, locally, are elongated parallel to $S_T$ and may enclose BtI, Ilm, Qz, Pl, Sil, and minor Zrn and Tur. Grt is mainly wrapped by a BtII-Sil-bearing foliation. Locally fine-grained Spl inclusions define Si trails in elongated Grt crystals (Fig. 5f), which are inclined to Se. Spl grains can be well preserved, with elongate shape and rational boundaries. In places, coronas of Wm, or BtIII overgrown by Chl, developed around Spl inclusions, both as reaction rims and as possible replacement of earlier Crd crystals. Generally, Bt (001) is parallel to $S_T$, but locally decussate texture with grains free of internal strain suggest that folded Bt is totally recrystallised and re-equilibrated at the end of $S_T$ development. The Fsp-rich domains, containing KfsI, Qz, and PlI may represent leucosomes transposed parallel to $S_T$, and intersected at a high angle by fractures filled with KfsII monocrystals. Granophyric textures are interstitial to Fsp grains defining $S_T$: similar structures are described in rocks that underwent partial melting at shallow depth (Holness, 2008). Post-kinematic Chl and Wm replaced Grt, Spl, Sil, and possible Crd.

#### 4.1.3. Ky-Spl-free metapelites

Bt, Sil, Pl, Kfs, and Qz display an SPO and locally LPO defining the $S_T$ fabric. In these rocks BtI porphyroclasts, wrapped by $S_T$, are in contact with Pl and BtII occur as fine-grained crystals defining the $S_T$ films together with Sil. $S_T$ is locally a crenulation cleavage, in which both foliations are defined by Bt and Sil SPO. Randomly oriented fibrolite locally replaced the prismatic Sil defining $S_T$, and overgrew microfold hinges. Bent BtI flakes in the microlithons, are either free of internal strain or still display marked undulose extinction. Locally, Ilm needles occur at Bt grain margins, suggesting exsolution of Ti induced by a late *T*-decrease. Coarse-grained Grt crystals wrapped by $S_T$ may be elliptical, with long axes parallel to $S_T$. Grt may enclose Bt, Ilm and rare Rt rimmed by Ilm. The internal foliation Si is inclined to Se at a high angle and may be discontinuous or asymptotic to Se. These relationships associated with the

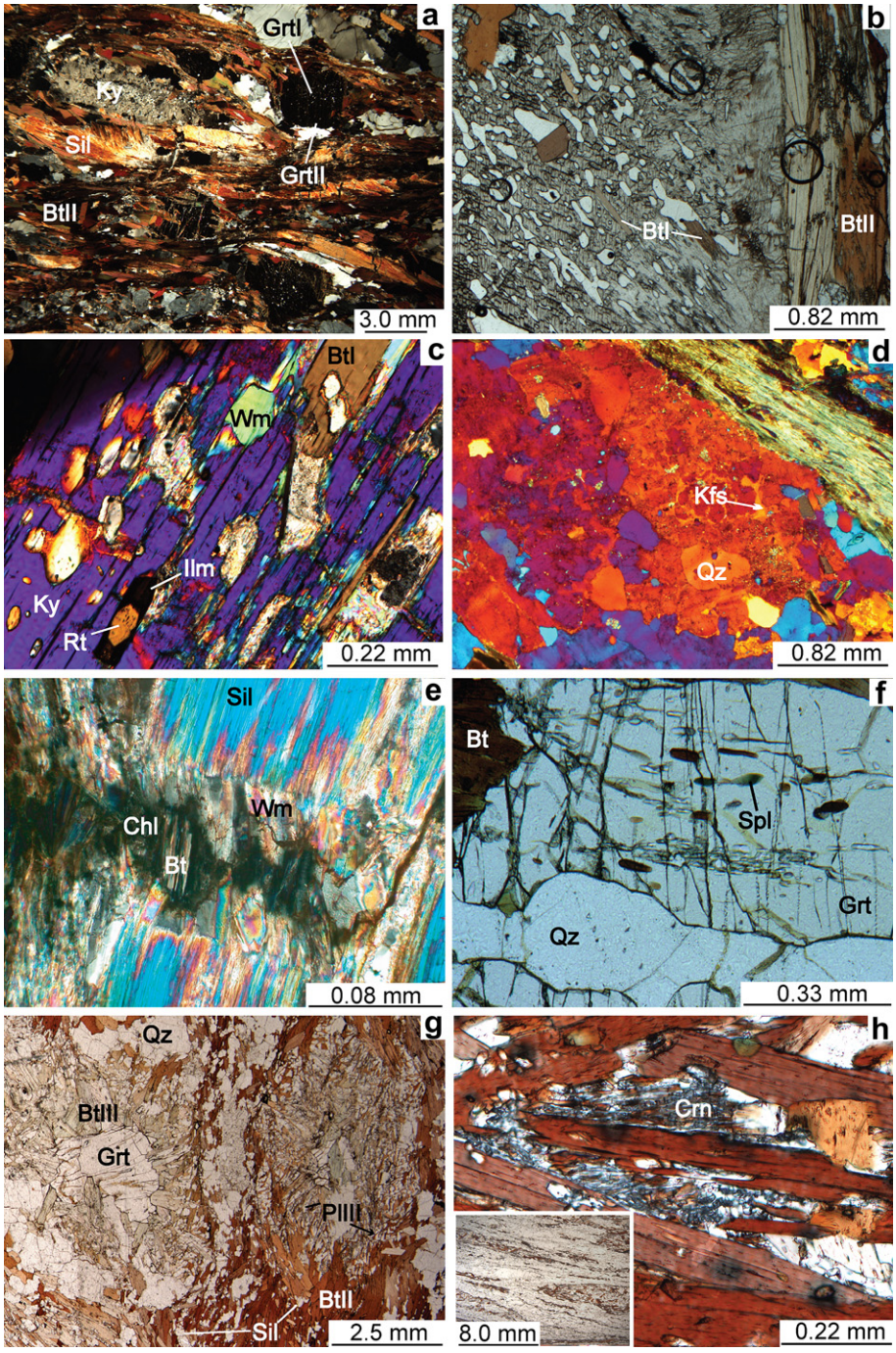


**Fig. 5.** Microstructures in metapelites; samples analysed for mineral chemistry are located in Fig. 2. a) Relict Ky and Grt are wrapped by $S_T$. Ky porphyroclast preserves an internal foliation, marked by Fsp, Qz and opaque minerals, at a high angle relative to the external $S_T$ foliation. Grt contains very fine-grained inclusions that are confined within the grain core (GrtI), whereas grain rims (GrtII) are inclusion-free. $S_T$ is marked by BtII and Sil; crossed polars (M59). b) Detail on the relationships between Si in Ky porphyroclast and Se (=$S_T$) in the matrix. BtI defines Si at high angle with respect to BtII defining $S_T$; plane polarised light (M59). c) Ky porphyroclast enclosing BtI, Rt rimmed by Ilm, and relict Wm; crossed polars and quarter-wave plate (M60). d) Kfs monocrystalline film interstitial to rounded Qz and Fsp crystals lying in Qz–Fsp-rich domains of $S_T$; crossed polars and quarter-wave plate (M60). e) Chl and Wm after Bt in the boudin necks of Sil defining $S_T$ and Sil lineation; crossed polars (M59). f) Trails of relict Spl are enclosed within syn-$S_T$ Grt porphyroblast; plane polarised light (90_5). g) Relict Grt is widely replaced by BtIII–PlIII symplectites that overgrow also Bt and Sil grains marking $S_T$; plane polarised light (90_4). h) Crn and Kfs replacing Sil and Bt defining the foliation in metapelites affected by a $D_{T+1}$ shear zone cutting the ca. 50 Ma old pegmatite at Blanket Mt.; in the inset an overview of the foliation affected by $D_{T+1}$ shear is shown; plane polarised light for both microphotographs (150488).

compositional crystal concentric zoning (see the following Mineral chemistry section), suggest a multistage growth of Grt, from pre- to syn-$S_T$. Grt is partially replaced by BtIII and PlIII symplectites that manifest a radial structure and overgrew $S_T$ (Fig. 5g): in these cases symplectite aggregates are coarse-grained and BtIII has a greenish pleochroism. BSE images show that a thin light rim occurs in the Grt (GrtIII) at the boundary with BtIII.

$S_T$-parallel domains, rich in Kfs, Pl and Qz, may represent transposed leucosomes. PlI shows growth twinning, and rarer deformation twinning and myrmekites developed at the Kfs rims.

Where $S_T$ is reactivated, during development of $D_{T+1}$ top-to-the-east shear zones, it is marked by Bt and fibrolite films alternating with Pl, Kfs and Qz-rich lithons. Rare relics of prismatic Sil are replaced by fibrolite and round aggregates of Bt and Pl probably replaced Grt. Crn and Kfs overgrew Sil and Bt films (Fig. 5h).

Greenschist facies minerals replacing Bt, Grt and Sil post-date $S_T$ and $D_{T+1}$. In general, Chl replaces Grt, and Chl, Wm and opaque minerals replace Bt, and Wm rims Sil. Late fractures ($D_{T+2}$) filled by Wm and Chl, are perpendicular to $S_T$ and intersect Sil, Pl and Grt grains. Chl and Wm locally define shear planes ($D_{T+2}$) at a low angle to $S_T$.

The micro-structural features of the three different types of metapelite can be synthesised by the following sequence of mineral assemblages:

1) Predating the development of $S_T$:
   a) In Ky-bearing metapelites: Grt + Pl + Qz + Bt + Ky + Rt with relics of Wm and St;
   b) In Spl-bearing metapelites: Spl + Bt + Grt + Qz;
   c) In Ky-Spl-free metapelites: Bt + Pl + Qz ± Sil ± Grt ± Rt.
2) Coeval with the development of $S_T$ in all types of metapelites: GrtII + PlII + BtII + Sil + Qz + Kfs + Ilm.
3) Postdating $S_T$ in Ky-bearing and Ky-Spl-free metapelites: BtIII + PlIII + KfsII + Qz (±GrtIII in Ky-Spl-free type).
4) During $D_{T+1}$ reactivation of $S_T$:
   a) In Ky-Spl-free metapelites: early) BtIV and fibrolite; later) Kfs, Crn and Ilm, which replaces the earlier phases.
   b) In Ky-bearing metapelites: a film of Qz, Ab, and Kfs crystallised from a late partial melt and is interstitial to the grains defining $S_T$.
5) During $D_{T+2}$:
   a) Late veins intersecting $S_T$ are filled by Chl + WmII ± pale Bt
   b) Shear planes contain Chl + WmII ± pale Bt
   c) Chl, sagenite, and fine-grained WmII partially replace Bt.

These mineral associations indicate that metapelites here underwent greenschist facies re-equilibration.

### 4.2. Metabasics

Metabasic rocks generally occur in boudins or layers and we recognise three types: massive granulites, Grt-bearing amphibolites and amphibolites. $S_T$ is generally defined by Amp, Pl and locally Bt.

#### 4.2.1. Granulites

These rocks, which form boudins wrapped by $S_T$, are generally massive and a local incipient foliation is defined by the SPO of a brown–green Amp. Grt, Cpx, AmpII, PlII and Qz form the granoblastic texture (Fig. 6a). Cpx, Grt and AmpII show rational grain boundaries. Grt forms poikiloblasts, which mainly include round grains of Qz, AmpI, Ilm, and minor PlI. Cpx is partially included in Grt rims or occurs in the matrix. Grt and Cpx are locally separated by a thin rim of emerald green Amp III and a symplectite of AmpIII and PlIII develops between AmpII and Grt. AmpII is zoned and shows a greener rim towards Grt; Spn rims Ilm grains enclosed in Grt. Locally, Chl replaces Amp at the outer edge.

#### 4.2.2. Grt-amphibolites

Like the granulites they occur as boudins, but show a dominant foliation ($S_T$), defined mainly by SPO (or locally LPO) of Bt, brown AmpII and minor Ilm and Qz. AmpI porphyroclasts and Grt are wrapped by $S_T$ (Fig. 6b and c), which also contains Ilm and Qz. Qz-rich lenses, with minor PlI and Cpx, are parallel to and are wrapped by an anastomosing $S_T$. PlI also occurs interstitially to AmpII grains or in granoblastic aggregates. Coarse-grained Grt is in mutual contact with PlI, Cpx and Amp; it may contain an Si inclined at a high angle to $S_T$ (Fig. 6c), marked by Pl, Qz and small grains of Amp. AmpII together with Pl and Qz occupies Grt strain shadows. Interstitial Qz grains occur between AmpII and PlII. Locally, coarse-grained Fe–Mg–Amp is wrapped by $S_T$ and is partially replaced by green AmpIII and Chl. Green AmpIII replaces Cpx and grew along rims and cleavages of AmpII; it in turn is overgrown by AmpIV. AmpIII and PlIII form symplectites at the edge of Grt. Spn rims Ilm and, if the replacement is complete, forms inequidimensional grains parallel to $S_T$. Chl overgrew the symplectite at the Grt grain boundaries, and together with sagenitic Rt, replaced Bt.

#### 4.2.3. Amphibolites

The amphibolites are generally foliated and only locally granoblastic. $S_T$ is mainly defined by SPO and LPO of coarse-grained Amp, rare Bt and millimetre-sized Pl, concentrated with minor Qz in $S_T$-parallel layers. The core of Amp grains (AmpI) is brownish while the rim (AmpII) is olive green (Fig. 6d). Pl defining $S_T$ shows a core (PlI) – rim (PlII) zoning. The sawtooth-shaped symplectitic boundary between AmpII and PlII consists of fine-grained AmpIII and PlIII (Fig. 6e). A light green actinolitic AmpIV rims the AmpIII and fills the fractures intersecting $S_T$ (Fig. 6d). Rare Cpx forms skeletal relict grains aligned parallel to $S_T$ in the Pl-rich domains, and round grains enclosed in Amp. Rare Bt grains are mainly parallel to $S_T$. Spn is abundant and partially replaces Rt, or forms crystals roughly parallel to $S_T$, which locally are millimetre size. Late Kfs edges Pl in symplectites or is interstitial between Amp and Pl lamellae; it fills fractures intersecting Amp and coarse-grained Spn. Within the late veins, Kfs is locally associated with actinolitic AmpIV and Pl grains that locally show deformation twinning, suggesting low-*T* deformation.

Micro-structural analysis of massive granulites allows recognition of the following time sequence for three mineral assemblages:

Grt + AmpI + Cpx + PlI + Qz + Ilm

AmpII + PlII + Qz

AmpIII + PlIII + Spn.

In foliated rocks the assemblage

AmpII + PlII + Qz ± Bt ± Rt/Spn

defines $S_T$.

Minerals that are relict with respect to $S_T$ occur in Grt-bearing amphibolites and amphibolites, respectively:

Grt + Cpx + AmpI + PlI + Qz

and

Cpx.

AmpIII + PlIII + Qz ± Spn postdates $S_T$; AmpIII is rimmed by actinolitic AmpIV; late veins are filled by Kfs.

### 4.3. Quartzites

Two foliations intersect at a low angle and the dominant one is generally defined by Sil, Ilm, Kfs and Qz SPO. Locally a shape foliation marked by Qz and KfsI is preserved in small domains bounded by the dominant foliation $S_T$ (Fig. 6f). Within this foliation re-oriented Wm is replaced by Sil and KfsII. Bt occurs as in porphyroclasts (BtI) or as thin rims (BtII) around relict Wm. Fibrolite occupies prismatic microsites suggesting that it is

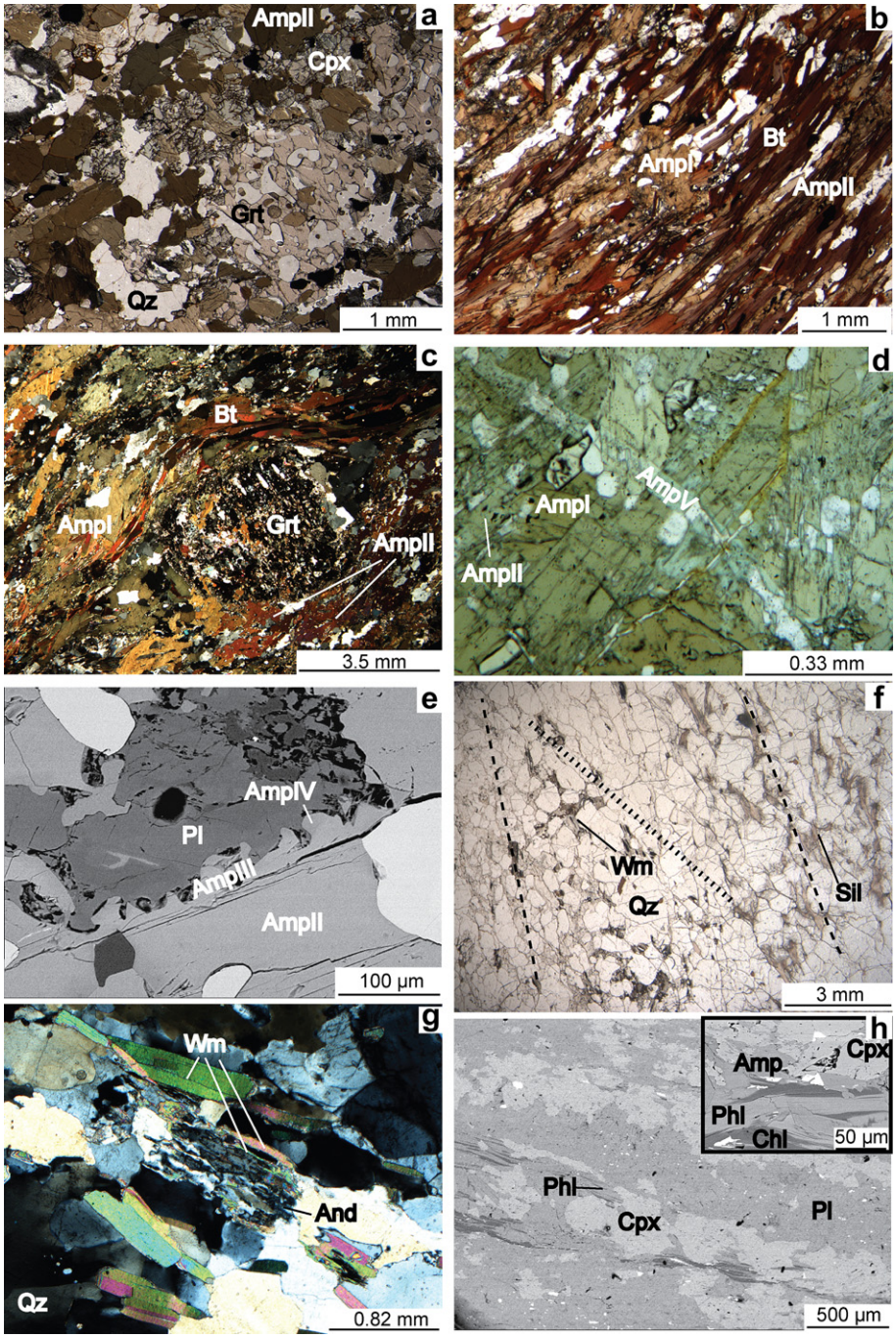


**Fig. 6.** Microstructures in metabasites, quartzites and calcsilicate rocks; samples analysed for mineral chemistry are located in Fig. 2. a) Granoblastic granulites with Grt porphyroblasts enclosing Amp, Pl and Qz. Grt has rational boundaries with Cpx and Amp of the matrix; thin reaction rims of new Amp and Pl symplectites develop at the margins of Grt and Cpx. White minerals are Qz and Fsp. Plane polarised light (04_054). b) Relict AmpI wrapped by $S_T$ marked by Bt and AmpII SPO, in Grt-bearing amphibolites; plane polarised light (M41). c) Relict Grt contains an internal foliation perpendicular to $S_T$, marked by Bt and AmpII (Grt-bearing amphibolites); crossed polars. d) AmpI rimmed by AmpII, marking $S_T$, both are cut by veins filled by AmpV in amphibolites; plane polarised light (90_6). e) AmpIII symplectites develop between AmpII grains and show AmpIV rims, in amphibolites; back scattered SEM image (90_6). f) Relict foliation marked by Bt and Wm is preserved at a small angle with the $S_T$ foliation marked by fibrous Sil (dashed line); dotted line indicates the Qz-shape foliation; plane polarised light (90_15). g) Pristine Wm marking $S_T$ in quartzites is locally overgrown by an And and Kfs polycrystalline aggregate, preserving relict Wm films; crossed polars. h) $S_T$ in calcsilicate rock marked by SPO of Cpx, Phl and Pl; in the inset Chl and Amp after Phl and Cpx; backscattered SEM images (90_18).

pseudomorphous after Ky or prismatic Sil (Fig. 6f); alternatively it is concentrated along shear surfaces together with Ilm trails. Some samples are Bt-free and the dominant foliation is marked by pristine Wm; these rocks may represent an early stage of fabric evolution during development of $S_T$. In this case the sole reaction texture is the replacement of Wm porphyroblasts by And and KfsIII (Fig. 6g). Greenschist re-equilibration is mainly associated with post-$S_T$ coronitic textures: new Wm rims Sil, and Chl rims Ilm; Chl, Wm and opaque minerals develop at the expense of Bt; new Wm occurs between And and Kfs.

These micro-structural features allow us to infer that the mineral association predating $S_T$ in quartzites was:

Wm + KfsI + Qz ± BtI + Ky or prismatic Sil (now fibrolite pseudomorphs).

**Table 3a**
Details on compositional variations in minerals from metapelites. Mineral composition have been determined using: i) Jeol, JXA-8200 electron microprobe (WDS, accelerating voltage of 15 kV, beam current of 15 nA) and Stereoscan 360 – ISIS 300 Oxford (EDS, accelerating voltage of 15 kV, sample current of 190 pA), both operating at the Earth Sciences Department of Milano University; ii) Jeol JXA-733 (WDS, accelerating voltage of 15 kV, beam current of 30 nA) and JSM 6400 SEM (EDS, accelerating voltage of 15 kV, beam current of 1.5 nA), both operating at the University of New Brunswick. Natural silicates have been used as standards and the results were processed for matrix effects using a conventional ZAF procedure. Proportional formulae have been calculated on the basis of: 22 oxygens for Bt and Wm, 12 oxygens for Grt, 8 oxygens for Fsp and 28 oxygens for Chl. $Fe^{3+}$ was determined only for Grt; cations are in a.p.f.u. = atoms per formula unit.

| Lithotype | Metapelites | | | Quartzites |
|---|---|---|---|---|
| | Ky-bearing (M59; M60) | Spl-bearing (90_5) | Ky-Spl-free (90_4; 90_9; 90_13; 160488B; 150488) | 90_15; 190488 |
| Bt | BtI: Ti = 0.32–0.56; $Al^{VI}$ = 0.51–0.96; $X_{Mg}$ = 0.39–0.48 | | BtI: Ti = 0.37–0.43; $Al^{VI}$ = 0.76–0.89; $X_{Mg}$ = 0.35–0.36 | |
| | BtII: Ti = 0.23–0.51; $Al^{VI}$ = 0.61–1.15; $X_{Mg}$ = 0.38–0.51 | BtII: Ti = 0.44–0.52; $Al^{VI}$ = 0.37–0.48; $X_{Mg}$ = 0.42–0.47 | BtII: Ti = 0.22–0.36; $Al^{VI}$ = 0.85–0.98; $X_{Mg}$ = 0.31–0.42 | Bt Syn-$S_T$: Ti = 0.16–0.33; $Al^{VI}$ = 0.70–1.39; $X_{Mg}$ = 0.54–0.59 |
| | BtIII: Ti = 0.14–0.36; $Al^{VI}$ = 0.75–1.02; $X_{Mg}$ = 0.41–0.49 | BtIII: Ti = 0.22–0.24; $Al^{VI}$ = 0.53–0.65; $X_{Mg}$ = 0.42–0.43 | BtIII: Ti = 0.00–0.03; $Al^{VI}$ = 1.10–1.37; $X_{Mg}$ = 0.51–0.55 | Bt replacing Wm: Ti = 0.19–0.30; $Al^{VI}$ = 0.63–0.99; $X_{Mg}$ = 0.54–0.62 |
| | BtIV: Ti = 0.09–0.22; $Al^{VI}$ = 0.57–0.91; $X_{Mg}$ = 0.29–0.49 | | Bt pre-$D_{T+1}$: Ti = 0.26–0.28; $Al^{VI}$ = 0.75–0.80; $X_{Mg}$ = 0.45–0.46 | |
| | | | Bt syn-$D_{T+1}$: Ti = 0.27–0.36; $Al^{VI}$ = 0.79–0.94; $X_{Mg}$ = 0.57–0.62 | |
| Grt | GrtI: Mg = 0.25–0.59; $Fe^{2+}$ = 1.99–2.24; Ca = 0.19–0.38; Mn = 0.05–0.20 | | GrtI: Mg = 1.06–1.07; $Fe^{2+}$ = 1.65–1.68; Ca = 0.21–0.22; Mn = 0.02–0.04 | |
| | GrtII: Mg = 0.39–0.57; $Fe^{2+}$ = 2.12–2.24; Ca = 0.13–0.30; Mn = 0.06–0.18 | Grt: Mg = 0.44–0.69; $Fe^{2+}$ = 1.91–2.26; Ca = 0.19–0.51; Mn = 0.00–0.05 | GrtII: Mg = 0.32–1.06; $Fe^{2+}$ = 1.65–2.24; Ca = 0.18–0.33; Mn = 0.05–0.10 | |
| | | | GrtIII: Mg = 0.42–0.77; $Fe^{2+}$ = 1.98–2.07; Ca = 0.17–0.20; Mn = 0.05–0.32 | |
| Pl | PlI: Ab = 0.57–0.60; An = 0.24–0.42; Or = 0.00–0.01 | Pl: Ab = 0.38–0.57; An = 0.41–0.62; Or = 0.00–0.02 | PlII: Ab = 0.68; An = 0.30; Or = 0.02 | |
| | PlII: Ab = 0.57–0.64; An = 0.34–0.42; Or = 0.00–0.01 | Pl post-$S_T$: An ca. 60% | PlIII: Ab = 0.60–0.61; An = 0.38–0.39; Or = 0.01 | |
| Wm | WmI: Si = 6.17–6.18; Ti = 0.02–0.04; $X_{Mg}$ = 0.17–0.19; $X_{Pg}$ = 0.08–0.09 | | | Pre-$S_T$: Si = 6.03–6.40; Ti = 0.00–0.21; $X_{Mg}$ = 0.31–0.51; $X_{Pg}$ = 0.03–0.07 |
| | WmII: Si = 6.02–6.38; Ti = 0.01–0.12; $X_{Mg}$ = 0.34–0.62; $X_{Pg}$ = 0.04–0.08 | Wm post-$S_T$: Si = 6.27–6.38; Ti = 0.00–0.11; $X_{Mg}$ = 0.20–0.39; $X_{Pg}$ = 0.02–0.03 | | Post-$S_T$: Si = 6.07–6.35; Ti = 0.01–0.03; $X_{Mg}$ = 0.26–0.45; $X_{Pg}$ = 0.02–0.04 |
| Kfs | Syn-$S_T$: Or = 0.79–0.90; An = 0.00; Ab = 0.09–0.21 | Syn-$S_T$: Or = 0.83–0.94; An = 0.00–0.01; Ab = 0.05–0.16 | Syn-$S_T$: Or = 0.92–0.94; An = 0.00; Ab = 0.05–0.08 | Pre-$S_T$: Or = 0.92-0.93; An = 0.00; Ab = 0.06–0.08 |
| | Monominerlic film: Or = 0.81–0.96; An = 0.00; Ab < 0.20 | | | Syn-$S_T$ recrystallised: Or = 0.88–0.92; An = 0.00; Ab = 0.08–0.10 |
| | Ab monomineralic film: Or = 0.00; An = 0.04; Ab = 0.96 | | | Post-$S_T$: Or = 0.94; An = 0.00; Ab = 0.06 |
| Chl | Chl-in Sil fractures: $X_{Mg}$ = 0.44–0.49; $Al^{tot}$ = 5.48–6.16 | Chl: $X_{Mg}$ = 0.50–0.52; $Al^{tot}$ = 5.05–5.25 | Chl-in Sil fractures: $X_{Mg}$ = 0.42; $Al^{tot}$ = 6.52 | |
| | Chl-in Grt fractures: $X_{Mg}$ = 0.25–0.29; $Al^{tot}$ = 5.32–5.82 | | Chl replacing Bt: $X_{Mg}$ = 0.46–0.54; $Al^{tot}$ = 5.20–5.90 | |
| | Chl replacing Bt: $X_{Mg}$ = 0.44–0.45; $Al^{tot}$ = 5.38–5.46 | | | |

**Table 3b**

Details on compositional variations in minerals from metabasics. Mineral composition have been determined using: i) Jeol, JXA-8200 electron microprobe (WDS, accelerating voltage of 15 kV, beam current of 15 nA) and Stereoscan 360 − ISIS 300 Oxford (EDS, accelerating voltage of 15 kV, sample current of 190 pA), both operating at the Earth Sciences Department of Milano University; ii) Jeol JXA-733 (WDS, accelerating voltage of 15 kV, beam current of 30 nA) and JSM 6400 SEM (EDS, accelerating voltage of 15 kV, beam current of 1.5 nA), both operating at the University of New Brunswick. Natural silicates have been used as standards and the results were processed for matrix effects using a conventional ZAF procedure. Proportional formulae have been calculated on the basis of: 22 oxygens for micas, 12 oxygens for Grt, 8 oxygens for Fsp and 28 oxygens for Chl 23 oxygens for Amp and 6 oxygens for Cpx. $Fe^{3+}$ was determined only for Grt and Cpx; cations are in a.p.f.u. = atoms per formula unit.

| Lithotype | Metabasics | | | | Calcsilicate |
|---|---|---|---|---|---|
| | Granulites | Grt-amphibolites | Amphibolites | | |
| Sample | 04-054 | M41 | 90_6 | 90_7 | 90_18 |
| Amp | M1: $Al^{tot}$ = 1.79−2.49; $Al^{VI}$ = 0.47−0.75; Ti = 0.13−0.25; Na(A) = 0.45−0.58; Na(B) = 0.00−0.10; $X_{Mg}$ = 0.36−0.39 | Pre-$S_T$: $Al^{tot}$ = 2.26; $Al^{VI}$ = 0.44; Ti = 0.17; Na(A) = 0.41; Na(B) = 0.03; $X_{Mg}$ = 0.57 | AmpI core: $Al^{tot}$ = 2.11−2.26; $Al^{VI}$ = 0.50−0.68; Ti = 0.11−0.20; Na(A) = 0.27−0.41; Na(B) = 0.00−0.09; $X_{Mg}$ = 0.58−0.61 | AmpI: $Al^{tot}$ = 0.85−1.72; $Al^{VI}$ = 0.28−0.60; Ti = 0.07−0.09; Na(A): 0.18-0.33; Na(B) = 0.00−0.07; $X_{Mg}$ = 0.75−0.79 | |
| | AmpII: $Al^{tot}$ = 2.14−2.52; $Al^{VI}$ = 0.41−0.66; Ti = 0.15−0.26; Na(A) = 0.49−0.58; Na(B) = 0.00−0.06; $X_{Mg}$ = 0.32−0.38 | Syn-$S_T$: $Al^{tot}$ = 0.90−2.31; $Al^{VI}$ = 0.27−0.78; Ti = 0.09−0.21; Na(A) = 0.14−0.33; Na(B) = 0.00−0.08; $X_{Mg}$ = 0.44−0.65 | AmpI rim: $Al^{tot}$ = 1.73−2.25; $Al^{VI}$ = 0.51−0.69; Ti = 0.10−0.16; Na(A) = 0.24−0.37; Na(B) = 0.00−0.09; $X_{Mg}$ = 0.59−0.63 | AmpII: $Al^{tot}$ = 0.32−0.62; $Al^{VI}$ = 0.13−0.23; Ti = 0.01−0.03; Na(A) = 0.01−0.08; Na(B) = 0.00−0.06; $X_{Mg}$ = 0.67-0.73 | |
| | AmpII rim: $Al^{tot}$ = 2.06−2.24; $Al^{VI}$ = 0.45−0.60; Ti = 0.16−0.26; Na(A) = 0.46−0.58; Na(B) = 0.00−0.08; $X_{Mg}$ = 0.33−0.37 | Post-$S_T$a: $Al^{tot}$ = 0.89−1.88; $Al^{VI}$ = 0.30−0.80; Ti = 0.00−0.09; Na(A) = 0.12−0.31; Na(B) = 0.00−0.08; $X_{Mg}$ = 0.39−0.65 | Symplectite: $Al^{tot}$ = 1.74−2.12; $Al^{VI}$ = 0.49−0.63; Ti = 0.14−0.18; Na(A) = 0.29−0.37; Na(B) = 0.01−0.07; $X_{Mg}$ = 0.58−0.62 | AmpIII: $Al^{tot}$ = 0.27−0.62; $Al^{VI}$ = 0.12−0.24; Ti = 0.00−0.03; Na(A) = 0.01−0.10; Na(B) = 0.00−0.08; $X_{Mg}$ = 0.58−0.72 | |
| | AmpIII: $Al^{tot}$ = 1.92−2.49; $Al^{VI}$ = 0.43−0.75; Ti = 0.12−0.19; Na(A) = 0.48−0.58; Na(B) = 0.00−0.03; $X_{Mg}$ = 0.32−0.35 | | AmpII: $Al^{tot}$ = 1.05−1.45; $Al^{VI}$ = 0.30−0.42; Ti = 0.07−0.12; Na(A) = 0.12−0.27; Na(B) = 0.00−00.7; $X_{Mg}$ = 0.65−0.69 | | Post-$S_T$: $Al^{tot}$ = 0.10−0.23; $Al^{VI}$ = 0.01−0.10; Ti = 0.01; $Na^{tot}$ < 0.10; $X_{Mg}$ = 0.85−0.90 |
| Grt | M1: Mg = 0.20−0.32; $Fe^{2+}$ = 1.60−1.82; Ca = 0.82−0.90; Mn = 0.07−0.15 | Pre-$S_T$: Mg = 0.23−0.57; $Fe^{2+}$ = 1.20−1.72; Ca = 0.79−0.97; Mn = 0.05−0.07 | | | |
| Pl | Enclosed in Grt: Ab = 0.63−0.67; An = 0.33−0.37; Or = 0.00 | Pre-$S_T$: Ab = 0.19−0.44; An = 0.55−0.81; Or = 0.00−0.01 | PlI: = Ab = 0.34−0.53; An = 0.45−0.65; Or = 0.01−0.02 | PlI core: Ab = 0.21−0.22; An = 0.78−0.79; Or = 0.00 | PlI Syn-$S_T$: Ab = 0.04−0.05; An = 0.95−0.96; Or = 0.00−0.02 |
| | In granoblastic matrix: Ab = 0.61−0.67; An = 0.31−0.38; Or = 0.01−0.02 In symplectites: Ab = 0.54−0.66; An = 0.33-0.45; Or = 0.00−0.01 | Syn-$S_T$: Ab = 0.26−0.66; An = 0.33−0.74; Or = 0.00−0.01 Post-$S_T$: Ab = 0.40−0.41; An = 0.58−0.59; Or = 0.00−0.01 | PlIII: Ab = 0.48−0.56; An = 0.42−0.35; Or = 0.01−0.02 PlIII: Ab = 0.64; An = 0.34−0.35; Or = 0.01 | PlI rim: Ab = 0.12−0.14; An = 0.86−0.88; Or = 0.00 | PlII Post-$S_T$: Ab = 0.41; An = 0.50; Or = 0.09 |
| Micas | | Syn-$S_T$ Bt: Ti = 0.11; $Al^{VI}$ = 0.56; $X_{Mg}$ = 0.37 | Syn-$S_T$ Bt: Ti = 0.09; $Al^{VI}$ = 1.74; $X_{Mg}$ = 0.55 | Post-$S_T$ Wm: Si = 6.18; Ti = 0.00; $X_{Mg}$ = 0.56; $X_{Pg}$ = 0.05 | Syn-$S_T$ Phl: Ti = 0.13−0.16; $Al^{VI}$ = 0.30−0.38; $X_{Mg}$ = 0.85−0.87 |
| Kfs | In symplectites: Or = 0.99; An = 0.00; Ab = 0.01 | | In symplectites: Or = 0.94−0.98; An = 0.00−0.02; Ab = 0.02−0.06 | In late veins: Or = 0.93−0.97; An = 0.00−0.03; Ab = 0.02−0.07 | Post-$S_T$: Or = 0.91; An = 0.00; Ab = 0.09 |
| Chl | | Post-$S_T$: $X_{Mg}$ = 0.46; $Al^{tot}$ = 5.19 | Post-$S_T$: $X_{Mg}$ = 0.53−0.56; $Al^{tot}$ = 4.94−5.03 | | Post-$S_T$: $X_{Mg}$ = 0.85−0.90; $Al^{tot}$ = 4.51−4.60 |
| Cpx | M1: $X_{Mg}$ = 0.52−0.58; $Al^{tot}$ = 0.07−0.11; Na = 0.02−0.06 | Pre-$S_T$: $X_{Mg}$ = 0.69-0.75; $Al^{tot}$ = 0.01-0.08; Na = 0.00-0.03 | Pre-$S_T$: $X_{Mg}$ = 0.69−0.73; $Al^{tot}$ = 0.01−0.12; Na = 0.01−0.03 | | Syn-$S_T$: $X_{Mg}$ = 0.90−0.93; $Al^{tot}$ = 0.01−0.03; Na = 0.00−0.01 |

During $S_T$ development the stable mineral assemblage was:

Sil + KfsII + Qz ± BtII.

Subsequently, domains that escaped deformation associated with Sil growth, in which metastable Wm is preserved, record the coronitic growth of:

And + KfsIII.

The last re-equilibration occurred under greenschist facies conditions, as indicated by the growth of:

Chl + WmII + opaque minerals.

### 4.4. Calcsilicate rocks

$S_T$ is defined by SPO of Cpx and Phl, which are concentrated in layers separating Pl and Qz-rich domains (Fig. 6h). In the Fsp-rich domains Pl dominates and forms coarse grains (PlI). Opaque minerals are prismatic and aligned in $S_T$. New fine-grained PlII is interstitial, Cpx has tremolitic Amp rims, and Mg-rich Chl replaces Phl along (001) cleavage. These micro-structural features suggest that the stable mineral assemblage during $S_T$ development was:

Cpx + PlI + Phl + Qz + opaque minerals.

It was replaced by the post-kinematic growth of:

Tr + Mg-Chl + PlII

indicating that a re-equilibration occurred under lower temperature (T) and pressure (P) conditions.

## 5. Mineral chemistry

Mineral compositions have been determined for selected micro-structural sites, chosen for their potential to reveal the trans-formation pathways accompanying fabric evolution, and to support thermobarometric estimates and P–T-d–t path reconstruction. Variations, synthesised below, are detailed in Tables 3a and 3b, which are supplemented by diagrams (Figs. 7–10). They show the compositional trends for mineral phases such as Bt, Grt, Cpx and Amp that are significant for thermobarometric estimates. Sample sites are located in Fig. 2.

### 5.1. Metapelites

Mineral compositions have been investigated for the three different types of metapelites as described in the microstructure (Table 3a). *Biotite* defining different fabric elements ($S_T$, $S_2$, or filling microfractures), has Mg- to Fe-Bt composition (Guidotti et al., 1975). It shows an increase in $Al^{VI}$ and a decrease in Ti, from pre- and syn-$S_T$ Bt to post-$S_T$ grains (Table 3a, Fig. 7a and b). Syn-$D_{T+1}$ Bt shows a remarkable Ti increase and high $X_{Mg}$ (Table 3a, Fig. 7c). *Garnet* zoning, from core to rim, is characterised by: an increase in Fe and Mn, a decrease in Mg and a local decrease in Ca (Table 3a; Fig. 8). An content of *plagioclase* decreases from andesine (syn-$S_T$) to oligoclase-albite composition (post-$S_T$) (Table 3a). *K-feldspar* shows a decrease in Ab content from syn-$S_T$ to post-$S_T$ grains (Table 3a); late monomineralic films are Ab or Kfs. *White mica* shows a very low Tschermak substitution (Table 3a) and the highest $X_{Mg}$ and Ti content are detected in grains replacing Bt. *Chlorite* plots in the ripidolite field (Hey, 1954) and its composition depends on bulk chemistry or micro-structural sites (Table 3a).

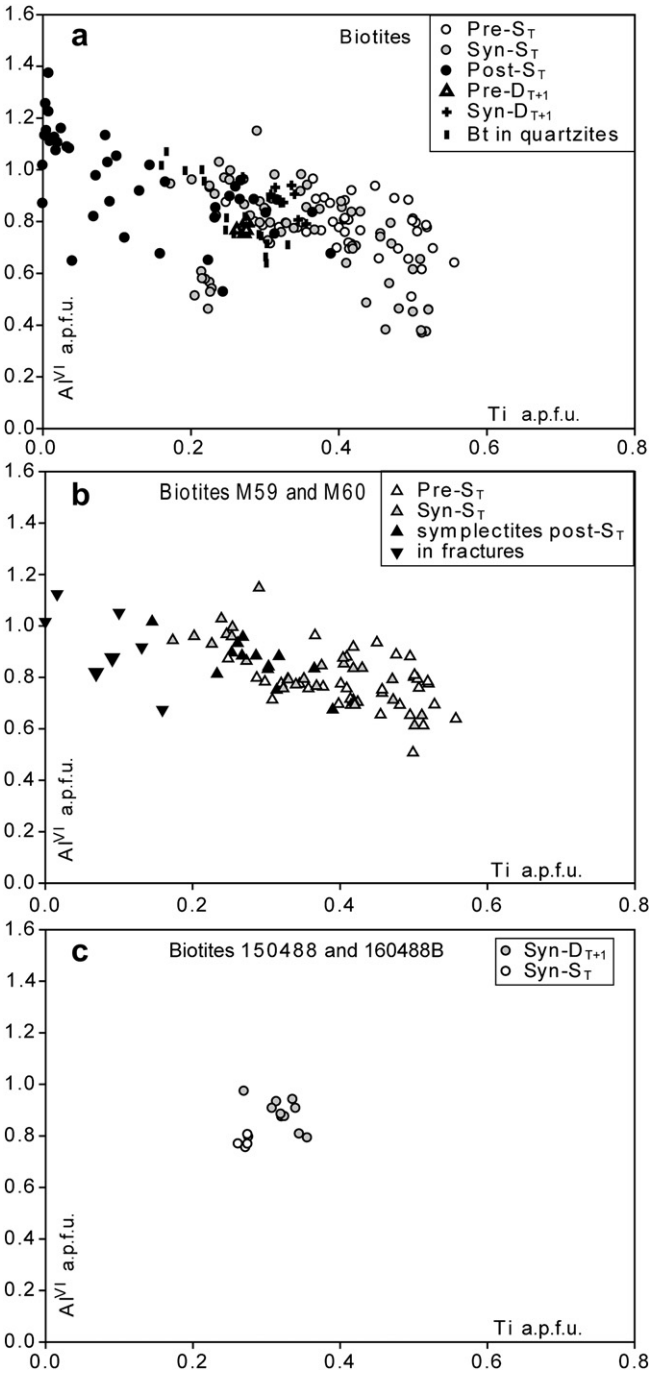


**Fig. 7.** Compositional variation of Bt in metapelites and quartzites. a) $Al^{VI}$ vs. Ti in biotites occupying different micro-structural sites from different metapelite samples and from quartzites. b) Detail of the compositional variations in Bt from Ky-bearing metapelites as a function of the micro-structural site. c) Compositions of Bt marking the foliation in $D_{T+1}$ shear zone (syn-$D_{T+1}$) and $S_T$ (syn-$S_T$); a.p.f.u. = atoms per formula unit.

### 5.2. Quartzites

In these rocks the main phases Bt, Fsp and Wm have been analysed. *Biotite* (Fig. 7a) is Mg-Bt (Guidotti et al., 1975); lower $Al^{VI}$ values characterise Bt rimming Wm porphyroclasts (Table 3a). *Feldspar*, mainly Kfs, has a quite homogeneous composition regardless of micro-structural site, as does Wm (Table 3a).

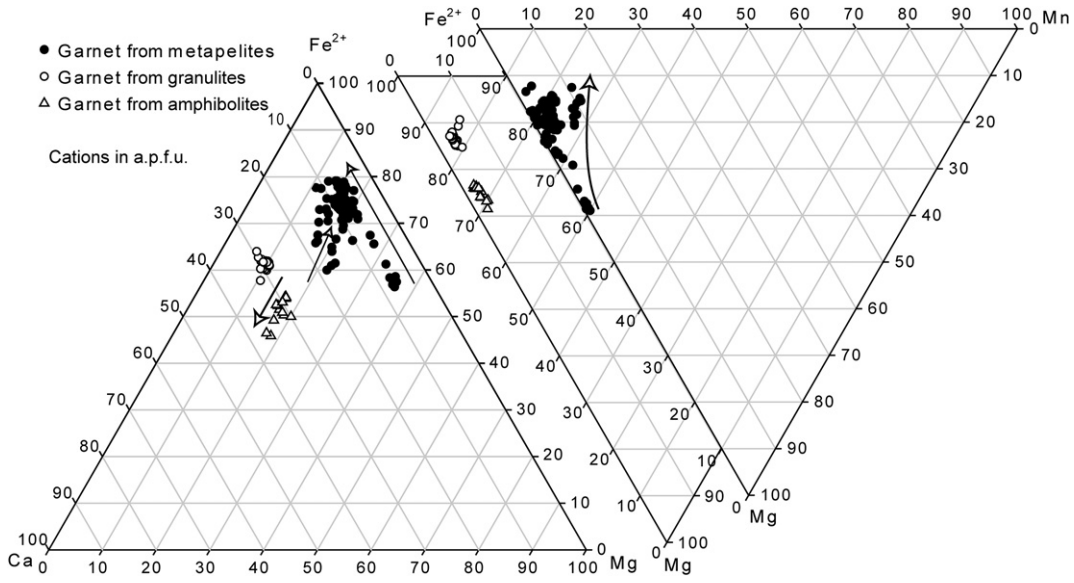


**Fig. 8.** Grt composition from metapelites, granulites and amphibolites; the arrows indicate the compositional trends from cores to rims; a.p.f.u. = atoms per formula unit.

### 5.3. Metabasics

Mineral compositions have been investigated for the three different types described in the microstructure (Table 3b). *Garnet* shows a moderate compositional zoning relatively to Grt from metapelites; a weak decrease of Mg, Mn and Fe and an increase in Ca content has been detected from core to rim only in Grt-bearing amphibolites (Fig. 8). *Clinopyroxene* is Di, according to Morimoto (1988), and its composition is controlled by bulk chemistry (Fig. 9, Table 3b). Cpx from granulites is quite homogeneous and characterised by higher contents of $Al^{tot}$ and Na, whereas it is zoned in amphibolites, where grain cores approach the composition of Cpx in the granulites. *Amphibole* composition from metabasics (Fig. 10, Table 3b), plots along the trend characterising Amp from the intermediate *P* rocks of Laird and Albee (1981). In granulites different generations of Amp are pargasitic. Ti content decreases from AmpI/II to AmpIII, while $Al^{tot}$, $Na^{tot}$ and $X_{Mg}$ are quite constant (Table 3b; Fig. 10a–c). In Grt-bearing amphibolites the composition of amphibole ranges between pargasitic and actinolitic; $Na^{tot}$, $Al^{tot}$ and Ti contents are higher in AmpI and II, than in AmpIII and AmpIV; $X_{Mg}$ is quite constant (Table 3b; Fig. 10a–c). In amphibolites (Table 3b and Fig. 10), $Na^{tot}$, $Al^{tot}$ and Ti content generally decreases from AmpI to AmpIV. The Ti vs. $Al^{tot}$ trend is shown in detail for various micro-structural sites in sample 90_6 (Fig. 10d). *Feldspars* are mainly Pl and are Kfs only in late fractures, or as an interstitial phase in amphibolites (Table 3b). An content is controlled by both bulk composition and micro-structural site: in granulites it increases from PlI/II to PlIII and Ab-rich Pl occurs as a reaction rim between PlIII and AmpIII; in Grt-bearing amphibolites An content decreases from PlI/II to PlIII, with lowest values in PlIII rimming PlII; in amphibolites (Table 3b) An content is strongly controlled by bulk composition and higher values are from sample 90_7, where a slight increase from core to rim suggests a late *T* increase. Generally $X_{An}$ decreases from core to rim, where is in equilibrium with AmpIV. *Biotite* in Grt-bearing amphibolites shows a lower Ti content and a comparable $X_{Mg}$ relative to Bt from metapelites; higher Ti content occurs in Grt-bearing amphibolites. Late *White mica* has a very low $Si^{4+}$ and $X_{Pg}$ contents (Table 3b). *Chlorite* plots in the field of ripidolite and pycnochlorite (Hey, 1954), the lowest values of $X_{Mg}$ occur in Grt-bearing amphibolites (Table 3b).

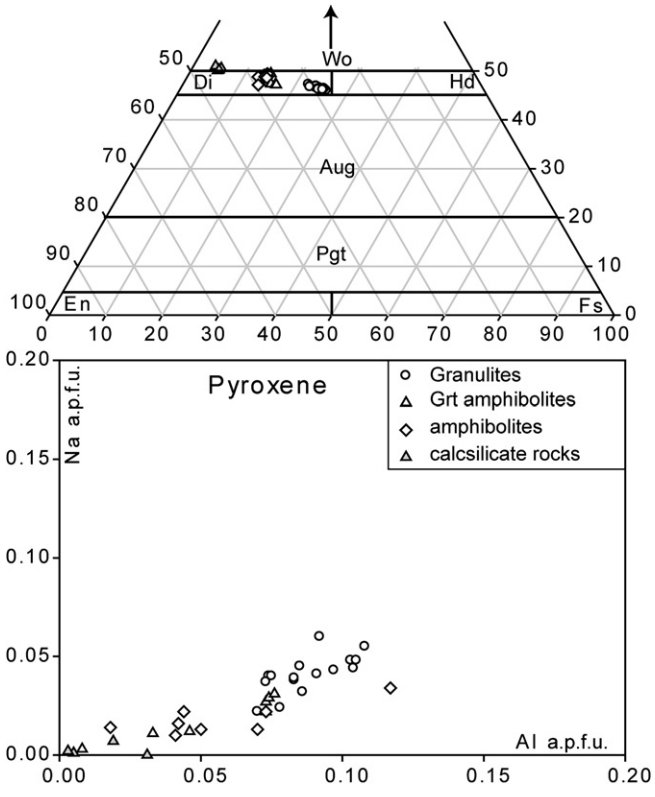


**Fig. 9.** Composition of Cpx in granulites, Grt-bearing amphibolites, amphibolites and calcsilicate rocks; a.p.f.u. = atoms per formula unit.

### 5.4. Calcsilicate rocks

In these rocks mineral composition has been determined for Cpx, Fsp, Phl, Amp and Chl (details in Table 3b). *Clinopyroxene* is Di (Morimoto, 1988) and it shows a higher $X_{Mg}$ and lower $Al^{tot}$ content than in the metabasics. *Feldspars* are An-rich Pl and Kfs; Kfs occurs as a reaction product at Pl rims. *Phlogopite* has a Ti content

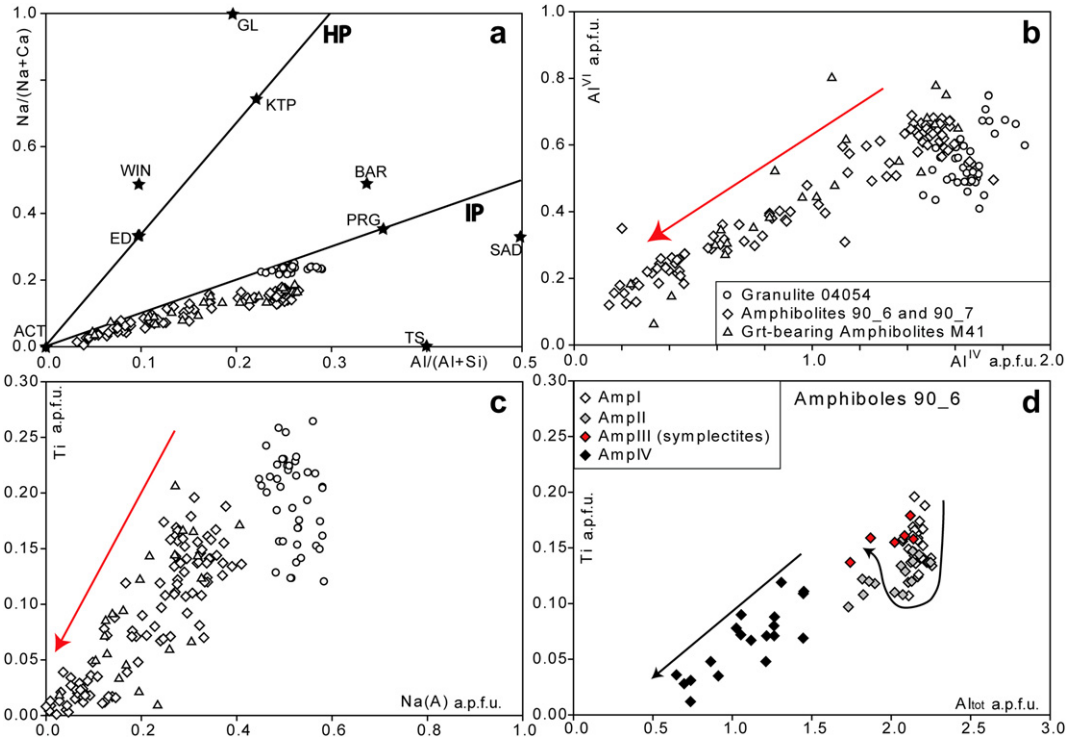


**Fig. 10.** a) Compositional range of Amp from granulites, Grt-bearing amphibolites and amphibolites. Stars locate the end-member compositions according to Leake et al. (1997): ACT = Actinolite; TS = Tschermakite; SAD = Sadanagaite; PRG = Pargasite; BAR = Barroisite; KTP = Katophorite; GL = Glaucofane; WIN = Winchite; ED = Edenite. Straight lines define high pressure (HP) and intermediate pressure (IP) Amp trends from Vermont (Laird and Albee, 1981). Analysed Amp plot along the IP trend. b) $Al^{IV}$ vs. $Al^{VI}$: the red arrow indicates the compositional trend from early to late Amp generation. c) Ti vs. Na(A): the red arrow as the same significance than in (b). d) Details of the compositional variation of Amp as a function of the micro-structural site in amphibolites (sample 90_6); a.p.f.u. = atoms per formula unit.

considerably lower than Bt from metapelites; *amphibole* is Tr or Act, and *chlorite* plots in the clinochlore field (Hey, 1954).

Compositional variation of mineral grains occupying different micro-structural sites (Table 3) ($X_{Mg}$ and Ti content in Bt, Ti and $Al^{tot}$ values in Amp, Al and Na content in Cpx, Grt compositional zoning, An content in Pl, $Si^{4+}$ content in Wm) indicates that decompression, generally associated with cooling, occurred during and after the development of the $S_T$ foliation. The syn-$D_{T+1}$ reactivation of $S_T$ is associated with a *T* increase, which is followed by a final cooling at very low *P*, as indicated by the $Si^{4+}$ content in syn-$D_{T+2}$ Wm in metapelites.

## 6. P–T estimates and metamorphic evolution

Micro-structural analysis indicates that the investigated rocks preserve evidence of superposed metamorphic re-equilibration and deformation (even in volumes as small as that of a thin section), and allowing the definition of paragenetic sequences in metapelites and metabasics. It also allows the identification of favourable sites, where microstructures suggest attainment of grain-scale equilibrium, for inferring PT conditions during each metamorphic re-equilibration. Following this approach, samples dominated by a single structural and metamorphic imprint, at thin section scale, yield internally coherent PT estimates, using independent thermobarometers. However, PT values derived using critical minerals such as Grt, in which the compositional zoning suggests a heterogeneous re-equilibration with the matrix assemblage, have been calculated using mineral pairs in mutual contact in carefully selected textural domains. Further, it has been demonstrated, under different metamorphic conditions, that mica and Amp grains associated with different fabric elements in the same rock, may have different chemical compositions, reflecting different intra- and inter-crystalline deformation mechanisms. This makes these minerals particularly suitable for estimation of physical conditions during the development of successive fabrics (e.g. Cimmino and Messiga, 1979; Lardeaux et al., 1983; Diella et al., 1992; Spalla, 1993; di Paola and Spalla, 2000; Gazzola et al., 2000).

PT conditions of each re-equilibration stage have been inferred using: a) the application of well calibrated independent thermobarometers; b) the comparison of natural assemblages with experimental univariant equilibria; c) calculation of univariant reaction curves using THERMOCALC by taking into account the end-member activity inferred using the AX program (Holland and Powell, 1998) based on specific mineral compositions. Thermobarometric estimates obtained using independent thermometers and barometers, are shown in Table 4 (metapelites) and Table 5 (metabasics and calcsilicates); calibrations have been applied, taking into account the best fit between the compositional range of mineral pairs in the different samples, and micro-structural sites. Estimated errors for each group of inferred PT values are shown in Tables 4 and 5.

### 6.1. Metapelites

#### 6.1.1. Pre-$S_T$

A *T* of ~700–850 °C for a *P* of 0.80–1.25 GPa has been estimated for pre-$S_T$ domains of Ky-bearing metapelites (pre-$S_T$ stage in Table 4). The occurrence of relict Wm and St older than the pre-$S_T$ assemblages constrains maximum *P* (*P*-max) at ≤1.3 GPa before pre-$S_T$, according to the reaction Grt + Ms = Bt + Ky + Qz (Fig. 11; Le Breton and Thompson, 1988). Minimum *P* (*P*-min) is

**Table 4**
Thermobarometric estimates obtained from metapelites using independent thermometers and barometers and referred to successive deformation stages. Legend: Ti in Bt = Ti content in Bt (Henry et al., 2005); Grt–Bt = Fe–Mg ion exchange reaction between Grt and Bt (1 = Perchuk et al., 1985; 2 = Perchuck and Lavrent'eva 1983; 3 = Bhattacharya et al., 1992; 4 = Ganguly and Saxena, 1984); GPBQ = equilibrium between Grt, Pl, Bt and Qz (1 = Hoisch, 1990; 2 = Wu et al., 2004); GASP = equilibrium between Grt, Pl, Als and Qz (1 = Newton and Haselton, 1981; 2 = Hodges and Spear, 1982; 3 = Ganguly and Saxena, 1984; 4 = Hodges and Crowley, 1985; 5 = Koziol, 1989); GRAIL = equilibrium between Grt, Rt, Als and Ilm (Bohlen et al., 1983); $Si^{4+}$ = $Si^{4+}$ content in Wm (Massonne and Schreyer, 1987).

| Lithotype | Sample | Stage | *T* (°C) | | | | | *P* (GPa) | | | | | | | |
|---|---|---|---|---|---|---|---|---|---|---|---|---|---|---|---|
| | | | Ti in Bt | Grt–Bt (1) | Grt–Bt (2) | Grt–Bt (3) | Grt–Bt (4) | GPBQ (1) | GPBQ (2) | GASP (1) | GASP (2) | GASP (3) | GASP (4) | GASP (5) | GRAIL | $Si^{4+}$ |
| Metapelites | Ky-bearing | M59 | Pre-$S_T$ | 716 ± 23 | | | | 1.24 ± 0.06 | | 1.17 ± 0.05 | 1.04 ± 0.05 | 1.09 ± 0.05 | 1.14 ± 0.05 | 1.22 ± 0.05 | 0.96 ± 0.03 | |
| | | | Syn-$S_T$ | 674 ± 38 | 698 ± 38 | | 641 ± 39 | 659 ± 50 | 0.58 ± 0.02 | 0.70 ± 0.01 | 0.54 ± 0.04 | 0.50 ± 0.02 | 0.48 ± 0.01 | 0.54 ± 0.03 | 0.63 ± 0.04 | | |
| | | | Post-$S_T$ | 630 ± 46 | | | | | | | | | | | | | ≤0.3 |
| | | | Syn-$D_{T+2}$ | 434 ± 78 | | | | | | | | | | | | | ($T \leq 512$) |
| | | M60 | Pre-$S_T$ | 724 ± 9 | 845 ± 33 | | 759 ± 30 | | 1.09 ± 0.22 | | 0.91 ± 0.02 | 0.80 ± 0.02 | 0.84 ± 0.03 | 0.92 ± 0.02 | 0.91 ± 0.02 | 0.99 ± 0.03 | |
| | | | Syn-$S_T$ | 702 ± 27 | | | | | 0.82 ± 0.03 | 0.81 ± 0.02 | 0.83 | 0.72 | 0.77 | 0.82 | 0.88 | | |
| | | | Post-$S_T$ | 682 | | | | | | | | | | | | | |
| | | | Syn-$D_{T+2}$ | <500 | | | | | | | | | | | | | |
| | Spl-bearing | 90_5 | Syn-$S_T$ | 730 ± 8 | 784 ± 38 | | 698 ± 27 | 732 ± 46 | 0.9 ± 0.13 | 0.76 ± 0.07 | 0.92 ± 0.15 | 0.77 ± 0.12 | 0.90 ± 0.19 | 0.90 ± 0.14 | 0.96 ± 0.10 | 0.87–0.94 | |
| | | | Post-$S_T$ | 608 ± 10 | | | | | | | | | | | | | |
| | Ky-Sp-free | 90_13 | Pre-$S_T$ | 689 ± 8 | | | | | | | | | | | | | |
| | | | Syn-$S_T$ | 632 ± 32 | | | | | | | | | | | | | |
| | | 90_9 | Syn-$S_T$ | 663 ± 15 | 706 ± 4 | | 669 ± 59 | 688 ± 11 | 0.86 ± 0.11 | 0.90 ± 0.08 | 0.88 ± 0.11 | 0.81 ± 0.10 | 0.83 ± 0.12 | 0.89 ± 0.12 | 0.92 ± 0.09 | | |
| | | 90_4 | Post-$S_T$ | | 628 ± 23 | 609 ± 19 | | | 0.48 ± 0.02 | | 0.48 ± 0.02 | 0.45 ± 0.02 | 0.46 ± 0.04 | 0.49 ± 0.02 | 0.58 ± 0.02 | | |
| | | 160488B | Pre-$D_{T+1}$ | 640 ± 3 | | | | | | | | | | | | | |
| | | 150488 | Syn-$D_{T+1}$ | 700 ± 14 | | | | | | | | | | | | | |

constrained by the Ky-Sil univariant equilibrium and maximum *T* (*T*-max) is limited by the dehydration melting reaction of Bt (Le Breton and Thompson, 1988; HGR field in Fig. 11). The occurrence of relict Wm and St enclosed in Ky and Grt, indicates that before pre-$S_T$ these rocks experienced a higher *P* and lower *T* metamorphic imprint, in the stability field of St (light grey field in Fig. 11 after Spear and Cheney, 1989), prior to undergoing the reaction Grt + Ms = Bt + Ky + Qz (Le Breton and Thompson, 1988; between AM and HGR fields in Fig. 11). In Spl-bearing metapelites, relicts of Spl enclosed in Grt suggest pre-$S_T$ $T > 800$ °C and $P < 0.9$ GPa, according to the univariant equilibrium Grt + Sil = Spl + Qz calculated with THERMOCALC (Holland and Powell, 1998; GR in Fig. 11). Pre-$S_T$ mineral relics in the Ky-Spl-free metapelites allow an estimate of pre-$S_T$ $T$ = 680–700 °C (Table 4).

### 6.1.2. *Syn-$S_T$*

*T* of 635–735 °C for *P* of 0.50–0.90 GPa, *T* of ~700–800 °C for *P* of 0.70–1.05 GPa and *T* of 600-730 °C for 0.80–1.00 GPa have been estimated for Ky-bearing, Spl-bearing and Ky-Spl-free metapelites, respectively. Syn-$S_T$ mineral assemblages in Spl-bearing metapelites are compatible with the Sil stability field, at *T* higher than that recorded in Ky-bearing and Ky-Spl-free metapelites (Fig. 11 and Table 4). Since the univariant equilibria Ms + Bt + Qz + V = L + Als (Ferri et al., 2009) and Ms + Ab + Qz = Kfs + Als + L (Le Breton and Thompson, 1988) are transgressed, some melt could have formed during pre- and syn-$S_T$ stages: related microstructures may not have been preserved because of the intense re-crystallisation during the development of $S_T$.

### 6.1.3. *Post-$S_T$*

These re-equilibration conditions were estimated at $T \sim 610$ °C, at *T* of 585–680 °C, at *T* of 590–650 °C for *P* of 0.45–0.60 GPa in Spl-bearing, Ky-bearing and Ky-Spl-free metapelites, respectively (Table 4). In Ky-Spl-free metapelites a pre-$D_{T+1}$ foliation, marked by Bt with a Ti content indicating $T \sim 640$ °C, is overprinted by syn-$D_{T+1}$ Bt with Ti content indicating $T \sim 700$ °C (Table 4).

In Ky-bearing metapelites the Ti content in BtIV (syn-$D_{T+2}$) is consistent with a *T*-decrease to values lower than 500 °C (Table 4); $P \leq 0.3$ GPa is estimated for the final cooling by the $Si^{4+}$ content in Ms filling the necks of Sil microboudins (syn-$D_{T+2}$; Table 4 and Fig. 11).

In summary, pre-$S_T$ PT conditions differ in Spl- and Ky-bearing metapelites and define two contrasted PT trajectories, which converge on a point under the PT conditions estimated for syn-$S_T$ assemblages. Syn-$S_T$ PT conditions span from granulite (GR) to amphibolite facies (AM). The P–T interval inferred from syn-$S_T$ mineral assemblages is wide, but the PT ranges characterising the different metapelite types are partially or totally overlapping (Table 4 and Fig. 11). This indicates that these assemblages quenched under different conditions in adjacent rock volumes suggesting that $S_T$ is a long lived fabric. The post-$S_T$ stage is on the low-T-side of the wet-granite solidus (Ab + Kfs + Qz + $H_2O$ = L; Le Breton and Thompson, 1988), and this suggests that partial melting did not take place. In contrast, the syn-$D_{T+1}$ (shear zones intersecting the pegmatite at Blanket Mt.) *T* conditions transgress the wet-granite solidus at low-*P* and, if $H_2O$ was available, partial melting could have occurred. This is consistent with the occurrence of microstructures interpreted as due to late low-P partial melting in metapelites, both immediately west of the Victor Creek fault and on Blanket Mt., and with the replacement of Crn + Kfs after Bt + Sil. According to reaction curves Grt + Bt = Chl + Ms and Bt + Als = Chl + Ms calculated with THERMOCALC (Holland and Powell, 1998), syn-$D_{T+2}$ conditions are at $T \leq 500$–550 °C and $P \leq 0.3$ GPa (Fig. 11).

**Table 5**
Thermobarometric estimates obtained from metabasites and calcsilicates using independent thermometers and barometers and referred to successive deformation stages. Legend: Ti in Amp = Ti content in Amp (Otten, 1984); Amp–Pl = NaSi–CaAl ion exchange reaction between Amp and Pl (1 = Holland and Blundy, 1994) and Al/Si ratio in Amp and Pl (2 = Plyusnina, 1982; 3 = Fershtater, 1990); Grt–Amp = Fe–Mg ion exchange reaction between Grt and Amp (Graham and Powell, 1984); Grt–Cpx = Fe–Mg ion exchange reaction between Grt and Cpx (Ellis and Green, 1979 after Powell, 1985); $Al^{tot}$ in Ca-Amp = $Al^{tot}$ content in Ca-Amp (Léger and Ferry, 1991); $Al^{tot}$ in Amp = $Al^{tot}$ content in Amp (1 = average between: Hammarstrom and Zen, 1986; Hollister et al., 1987; Johnson and Rutherford, 1989; 2 = Schmidt, 1992); Grt–Pl–Cpx = equilibrium between Grt, Pl, Cpx and Qz (1 = Moecher et al., 1988; 2 = Eckert et al., 1991); Grt–Pl–Amp = equilibrium between Grt, Pl, Amp and Qz (Kohn and Spear, 1990); GRIP = equilibrium between Grt, Rt, Ilm, Pl and Qz (Bohlen and Liotta, 1986).

| Lithotype | | Sample | Stage | *T* (°C) | | | | | | *P* (GPa) | | | | | | | | |
|---|---|---|---|---|---|---|---|---|---|---|---|---|---|---|---|---|---|---|
| | | | | Ti in Amp | Amp-Pl (1) | Grt–Amp | Grt–Cpx | $Al^{tot}$ in Ca-Amp | Amp-Pl (2) | $Al^{tot}$ in Amp (1) | $Al^{tot}$ in Amp (2) | Grt–Pl–Cpx (1) | Grt–Pl–Cpx (2) | Grt–Pl–Amp | GRIP | Amp-Pl (2) | Amp-Pl (3) | $Al^{tot}$ in Ca-Amp |
| Metabasics | Granulites | 04-054 | M1 | 769 ± 47 | 748 ± 16 | 782 ± 36 | 745 ± 23 | | | | | 1.17 ± 0.08 | 0.95 ± 0.05 | 1.00 ± 0.05 | 1.14 ± 0.08 | | | |
| | | | AmpII | 802 ± 37 | | | | | | | | | | | | | | |
| | | | AmpII rim | 804 ± 32 | | | | | | | | | | | | | | |
| | | | AmpIII sympl | 720 ± 28 | 723 ± 31 | | | | | 0.69 ± 0.14 | 0.76 ± 0.13 | | | | | | | |
| | Grt-amphibolites | M41 | Pre-$S_T$ | 750 | | | 716 ± 25 | | | | | 0.95 ± 0.05 | 0.90 ± 0.03 | | | | | |
| | | | Syn-$S_T$ | 715 ± 43 | ~750 | | | | | | 0.56 ± 0.23 | | | | | | | |
| | | | Post-$S_T$1 | 615 ± 33 | 638 ± 37 | | | | | | 0.31 ± 0.17 | | | | | | | |
| | | | Post-$S_T$2 | | | | | | 500–550 | | | | | | | <0.2 | ≤0.2 | |
| | Amphibolites | 90_6 | AmpI (Syn-$S_T$) | 726 ± 24 | 715 ± 14 | | | | | 0.68 ± 0.08 | 0.73 ± 0.02 | | | | | | | |
| | | | AmpI rim (Syn-$S_T$) | 698 ± 21 | 713 ± 6 | | | | | 0.65 ± 0.08 | 0.66 ± 0.07 | | | | | | | |
| | | | sympl post AmpI | 735 ± 16 | 703 ± 7 | | | | | 0.59 ± 0.10 | 0.65 ± 0.08 | | | | | | | |
| | | | Post-$S_T$1 | 595 ± 70 | 591 ± 64 | | | | | | 0.29 ± 0.07 | | | | | | | |
| | | | Post-$S_T$2 | | | | | | 500–550 | | | | | | | <0.2 | ≤0.2 | |
| | | 90_7 | AmpI | 629 ± 16 | 657 ± 18 | | | | | | | | | | | | | |
| | | | AmpII | 570 ± 38 | | | | | | | | | | | | | | |
| | | | AmpIII | | | | | <500 | | | | | | | | | | <0.35 |
| | Calcsilicates | 90_18 | Post-$S_T$ | | | | | <550 | | | | | | | | | | <0.2 |

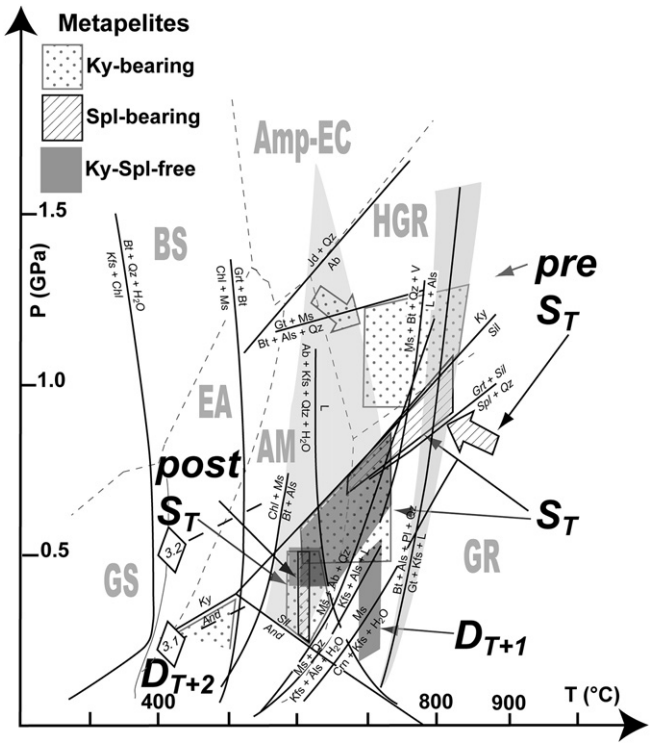


**Fig. 11.** P–T-d–t history inferred from PT-estimates for different metapelite types (see legend). Reaction curves labelled in italics are calculated with THERMOCALC (Holland and Powell, 1998) on the basis of end-member activities. Reaction curves labelled with regular characters are from the literature: Jd + Qz = Ab, Ms = Crn + Kfs + $H_2O$ and Ms + Qz = Kfs + Als + $H_2O$ (Spear, 1993); Ms + Bt + Qz = L + Als (Ferri et al., 2009); Ab + Kfs + Qz + $H_2O$ = L, Bt + Als + Pl + Qz = Grt + Kfs + L, Ms + Ab + Qz = Kfs + Als + L, and Grt + Mu = Bt + Als + Qz (Le Breton and Thompson, 1988). 3.1 and 3.2 labelling thick dashed lines are Si-isopleths in Wm (Massonne and Schreyer, 1987). Metamorphic facies (Ernst and Liou, 2008): GS = greenschist; EA = epidote – amphibolite; BS = blueschist; AM = amphibolite; Amp-EC = amphibole-bearing eclogite; HGR = high pressure granulite; GR = granulite. The light grey fields correspond to the stability field of staurolite (Spear and Cheney, 1989) and to the PT interval of Bt dehydration melting (Le Breton and Thompson, 1988). Stripped and dotted arrows indicate the most likely pre-$S_T$ trajectories.

### 6.2. Metabasics

#### 6.2.1. Massive fabric

The massive granoblastic fabric in granulites occurs in mafic boudins wrapped by $S_T$ and has been interpreted therefore as predating $S_T$. In these rocks, because no foliated fabric developed during the subsequent mineral re-equilibrations, their geometric and kinematic relationships with $S_T$ in the country rock cannot be inferred. Pre-$S_T$ PT conditions (Table 5) have been estimated at $T$ values of 720–820 °C for $P$ of 0.90–1.25 GPa. $Al^{tot}$ content in AmpIII, from the Grt-free symplectitic assemblage, suggests a $P$ of 0.55–0.90 GPa for $T$ of 690–755 °C, for this re-equilibration stage, as indicated by the Ti content of AmpIII and the Amp and Pl thermometer (Table 5).

#### 6.2.2. Foliated fabric

*Pre-$S_T$*: In Grt-bearing amphibolites $T$ 690–750 °C for $P$ of 0.85–1.00 GPa have been estimated (Table 5).

*Syn-$S_T$*: $T$ of 670–760 °C for $P$ of 0.35–0.80 GPa and $T$ of 675–750 °C for $P$ of 0.50–0.75 GPa have been obtained in Grt-bearing amphibolites and amphibolites, respectively (details in Table 5).

*Post-$S_T$*: we recognise two stages of post-$S_T$ re-equilibration in metabasics which are hereafter referred to as Post-$S_T$1 and Post-$S_T$2. Post-$S_T$1 re-equilibration in Grt-amphibolites occurred at $T$ of 580–675 °C and $P$ of 0.15–0.50 GPa; the subsequent re-equilibration (post-$S_T$2) conditions occurred at $T \leq$ 500–550 °C and $P <$ 0.2 GPa (Table 5).

In amphibolites post-$S_T$1 re-crystallisation occurred at $T$ of 525–675 °C for $P$ of ca. 0.30 GPa; the conditions for development of the last assemblage (post-$S_T$2) are estimated at $T$ = 500 and 550 °C and $P \leq$ 0.2 GPa (Table 5). Locally most re-equilibrated massive amphibolites (e.g. sample 90_7 in Table 5) contain zoned Amp giving $P$ and $T$ values compatible with those characterising the final stages of metamorphic re-equilibration (post-$S_T$1 and post-$S_T$2). These rocks have a Ca content in Pl and Amp high enough to invalidate the application of the barometers based on the $Al^{tot}$ content of Amp; in such a Ca-rich system, the thermobarometer calibrated by Léger and Ferry (1991) is applied to estimate $T <$ 500 °C and $P <$ 0.35 GPa from the retrograde AmpIII.

In calcsilicates the application of the same thermobarometer (Léger and Ferry, 1991) on the retrograde post-$S_T$ Amp yields $T <$ 550 °C and $P <$ 0.2 GPa. This PT interval agrees with the PT space (inset in Fig. 12) outlined by the reaction curves calculated with THERMOCALC (Holland and Powell, 1998; Phl + Di + Qz = PlII + Tr and PlI + Phl = PlII + Amp) and with the Chl-out curve (Liou et al., 1974).

In summary, the pre-$S_T$ stage in metabasics is recorded in granulites and Grt-amphibolites by the assemblage Grt–Cpx–Pl–Amp–Qz indicating $P$ higher than those of the Grt-in curve and $P$ and $T$ lower than the Pl-out curve (HGR in Fig. 12: Liou et al., 1996). The estimated syn-$S_T$ conditions for Grt-amphibolites and

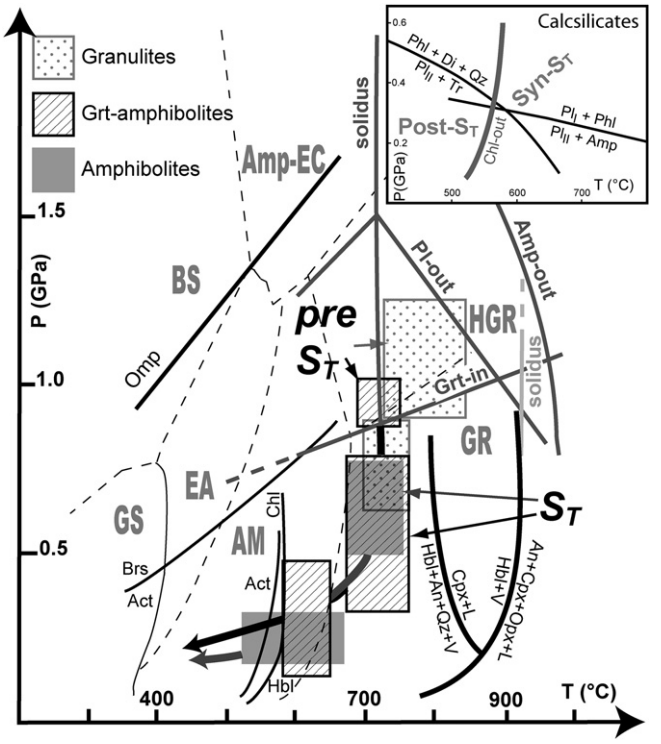


**Fig. 12.** P–T-d–t history inferred from PT-estimates on different types of metabasics (see legend). Chl-in (Liou et al., 1974); Brs/Act transition (Ernst, 1979); Act/Hbl transition (Moody et al., 1983); Omp-in (Poli and Schmidt, 1995); Pl-out, Amp-out, Grt-in, and wet basalt solidus (Liou et al., 1996); dry basalt solidus (Rushmer, 1993); Hbl + An + Qz + V = Cpx + L and Hbl + V = An + Cpx + Opx + L (Ellis and Thompson, 1986). Metamorphic facies (Ernst and Liou, 2008): GS = greenschist; EA = epidote – amphibolite; BS = blueschist; AM = amphibolite; Amp-EC = amphibole-bearing eclogite; HGR = high pressure granulite; GR = granulite. Inset: stability fields of syn-$S_T$ and post-$S_T$ mineral assemblages in calcsilicate rocks. Equilibria Phl + Di + Qz = PlII + Tr and PlI + Phl = PlII + Amp are calculated with THERMOCALC (Holland and Powell, 1998) on the basis of end-member activities. Chl-Out is after Liou et al. (1974).

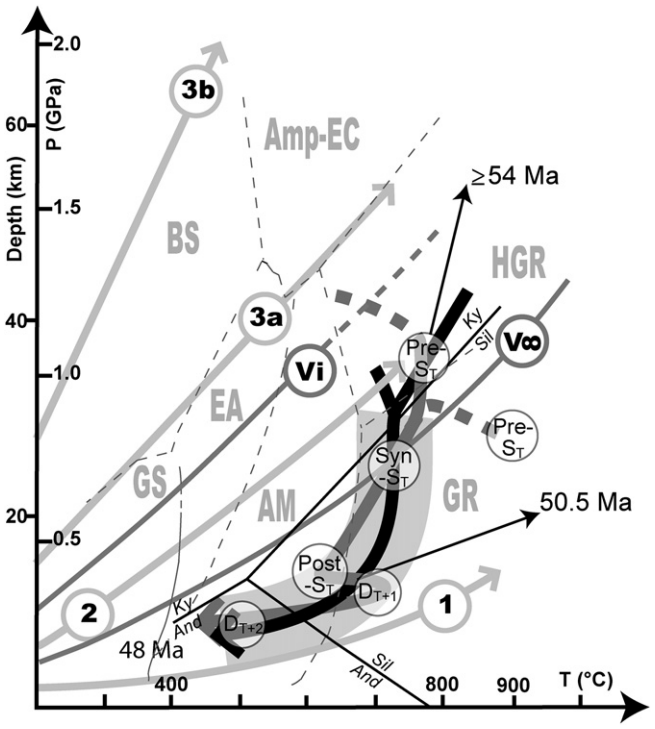


**Fig. 13.** PT paths inferred for the metapelites (grey) and metabasics (black); the shaded area represents the variation between minimal and maximal estimated *T* values in metabasics. Geotherms: 1) near spreading ridge or volcanic arc, 2) normal gradient of old plate interior, 3a) "warm" subduction zones, 3b) cold subduction zones (Cloos, 1993); Vi = stable and V∞ = relaxed geotherms (England and Thompson, 1984) for continental crust.

amphibolites occur at *P* lower than the Grt-in curve (Liou et al., 1996) and at lower *T* than the Hbl + An + Qz + V = Cpx + L equilibrium (Ellis and Thompson, 1986), consistent with the observed Grt-, Cpx- and melt-free assemblages (GR in Fig. 12). These conditions are partially overlapped by PT estimates obtained by AmpIII and PlIII coronas in granulites, indicating that the last are the coronitic equivalents of syn-$S_T$ assemblages in foliated rocks. Post-$S_T$ re-equilibration stages occurred under amphibolite facies (post-$S_T$1) towards greenschist facies (post-$S_T$2) conditions (AM and GS in Fig. 12), and intersect the Chl-in curve (Liou et al., 1974) as indicated by Chl occurrence in retrograde assemblages. A final low-*T* – low-*P* retrogradation occurred in a PT interval equivalent to that of syn-$D_{T+2}$ assemblages in metapelites.

## 7. Discussion and conclusions

Meso- and micro-structural and petrologic analysis of a transect from the northern slope of Blanket Mt. to the plateau immediately south of Greenbush Lake (Figs. 1 and 2), reveal that despite the homogeneous appearance of the transposition foliation $S_T$, not all of the rocks share a common pre-$S_T$ geological history. This is evident in microscopic to metre-sized relicts in the form of, for example, boudins wrapped by the $S_T$ and mineral inclusions that have different PT signatures: the resulting PT trajectories, predating the development of the Sil-bearing $S_T$, are contrasted.

P–T-d–t paths reconstructed for metapelites and metabasics are summarised in Fig. 13. They show that the exhumation of this portion of Cordilleran deep crust occurred under an anomalously high thermal regime, compatible with extensional-tectonics-induced lithospheric thinning. *T*/Depth (Table 6) ratios show an increase going from pre-$S_T$ to post- $S_T$ times in both metapelites and metabasics. The pre-$S_T$ thermal gradient is lower than the normal geothermal gradient of 25 °C $km^{-1}$ (e.g. Cloos, 1993), whereas the syn-$S_T$ and post-$S_T$ gradients are higher than the normal gradient, approaching 60 °C $km^{-1}$ during post-$S_T$ times. The whole PT-retrograde path is characterised by a *T*/*P* ratio (Table 6), higher than the maximally relaxed geotherm after continental collision (V∞ of England and Thompson, 1984), that increases from $D_T$ to $D_{T+2}$ stages (Fig. 13), indicating that extension accompanied by exhumation was ongoing throughout this time.

Wm and St, which predate the Ky-bearing assemblage in metapelites, are interpreted as relics of an earlier Barrovian metamorphic imprint, which is compatible with the thermal gradient characterising a thickened crust during a mature collision. This could represent the accretion of the allochthonous terranes onto the western palaeo-margin of North America (Laurentia) that may have taken place sometime between Jurassic and Cretaceous time (e.g. Monger et al., 1982; Gibson et al., 2008). The pre-$S_T$ stage in Ky-bearing metapelites, compatible with the pre-$S_T$ signature in metabasics, may reflect thermal relaxation at a deep structural level, in a collision-thickened continental crust. Re-equilibration under high *T*- and high *P*-conditions postdating St-bearing assemblages are also detected in Grt-bearing Ged–Crd boudins from the southern part of the dome (Norlander et al., 2002).

The ca. 54 Ma Ky-bearing pegmatites (Johnston et al., 2000) in the Blanket area indicate that the pre-$S_T$ Ky-bearing assemblage in metapelites can be 54 Ma or older. The pegmatites infill boudin necks within $S_T$ (Johnston et al., 2000), suggesting that the Ky-bearing assemblage is coeval with at least a part of the transposition history ($D_T$). Subsequently most Ky was replaced by Sil,

**Table 6**
Average P/T and T/Depth ratios estimated for the re-equilibration stages in the metapelites and metabasics based on an average density for the continental crust of ~2.9 $gcm^{-3}$, according to Spear (1993).

| Lithotype | | Stage | Av *T* (°C) | Av *P* (GPa) | Av *P*/*T* (GPa/°C) | Av *T*/depth (°C/km) |
|---|---|---|---|---|---|---|
| Metapelites | Ky-bearing | Pre-$S_T$ | 770 | 1.1 | $1.43 \times 10^{-3}$ | 20.01 |
| | | Syn-$S_T$ | 673 | 0.65 | $0.97 \times 10^{-3}$ | 29.73 |
| | | Post-$S_T$ | 610 | 0.39 | $0.64 \times 10^{-3}$ | 44.91 |
| | | $D_{T+2}$ | <500 | <0.4 | $0.8 \times 10^{-3}$ | 35.98 |
| | Spl-bearing | Pre-$S_T$ | >800 | <0.9 | $>1.04 \times 10^{-3}$ | >25.52 |
| | | Syn-$S_T$ | 745 | 0.84 | $1.13 \times 10^{-3}$ | 25.47 |
| | Ky-Spl free | Syn-$S_T$ | 673 | 0.63 | $0.94 \times 10^{-3}$ | 30.67 |
| | | Post-$S_T$ | 610 | 0.39 | $0.64 \times 10^{-3}$ | 44.91 |
| | | $D_{T+1}$ | 700 | 0.4 | $0.57 \times 10^{-3}$ | 50.25 |
| Metabasics | Granulites | Pre-$S_T$ | 783 | 1.08 | $1.37 \times 10^{-3}$ | 20.82 |
| | | Syn-$S_T$ | 765 | 0.7 | $0.91 \times 10^{-3}$ | 31.38 |
| | Grt-amphibolites | Pre-$S_T$ | 720 | 0.95 | $1.32 \times 10^{-3}$ | 21.76 |
| | | Syn-$S_T$ | 720 | 0.56 | $0.77 \times 10^{-3}$ | 36.92 |
| | | Post-$S_T$ | 615 | 0.31 | $0.50 \times 10^{-3}$ | 56.96 |
| | Amphibolites | Syn-$S_T$ | 713 | 0.61 | $0.86 \times 10^{-3}$ | 33.29 |
| | | Post-$S_T$ | 600 | 0.25 | $0.42 \times 10^{-3}$ | 68.91 |

which generally defines $S_T$. Syn-kinematic mineral assemblages and the thermobarometric estimates indicate that $S_T$ formed and was reworked over a range of *P*-conditions varying between 1.1 and 0.5 GPa. This makes the transposition history compatible with a continuous deformation event (Williams and Jiang, 2005), still acting during the exhumation of the Cordilleran deep crust across different structural levels (from 30 to 15 km depth). This extended history of transposition is consistent with the channel flow model proposed by Williams and Jiang (2005) and Kuiper et al. (2006). The greater part of the exhumation has been accomplished after the transgression of V∞ (Fig. 13) indicating a thermal state higher than that consequent to a continental collision. The observed state is consistent with the existence of an additional heat supply, such as that generated by asthenospheric upwelling during lithospheric thinning.

The pre-$S_T$ PT conditions in Spl-bearing metapelites are incompatible with the Cordilleran collision history because they testify to a geothermal gradient higher than the maximally relaxed geotherm after continental collision (V∞ in Fig. 13: England and Thompson, 1984), consistent with a thinned lithosphere. If the old ages of ca. 860–750 Ma (based on whole rock Rb/Sr data of Duncan, 1984), for migmatisation of the southern part of the dome, are still considered reliable, this high thermal regime could be interpreted as a product of lithospheric thinning during the initial break up of Rodinia (Dalziel, 1997; Li et al., 2008), leading to the development of the western Laurentian passive margin. Consistent ages of intraplate igneous activity are ~724 Ma for the Mount Grace syenitic gneiss protoliths (Crowley, 1997), and ~740 Ma for the Mount Copeland syenite gneiss protoliths (Okulitch, 1984). Deposition of the Windermere Supergroup (e.g. Eisbacher, 1985) and possibly part of the cover sequence would also be compatible with this interpretation, which should be tested by determination of the absolute age of the micro-structural relicts.

The contrasting pre-$S_T$ PT conditions are followed by homogeneous assemblages resulting from re-equilibration of rocks of different bulk composition during $S_T$ development (Sil-bearing assemblages in metapelites). Syn-$S_T$ assemblages mainly belong to the granulite facies, and deformation responsible for $S_T$ development acted as a mechanical and chemical homogeniser that largely erased the previous geological record. PT conditions of some coronitic structures preserved in metabasics are compatible with those estimated for mineral assemblages defining $S_T$ in metapelites and foliated metabasics (see Tables 4 and 5). The evidence suggests that some granulitic metabasic boudins may have been essentially rigid during the transposition: they are the most suitable and reliable recorder of the pre-transposition geological history. Therefore the randomly distributed exotic remnants may represent vestiges of tectonometamorphic units with different geological histories. In this case, the contrasted pre-$S_T$ imprints may represent remnants of the history of the western Laurentian passive margin as well as of the Cordilleran subduction zone (geotherm 3a in Fig. 13), widely obliterated by the late Cordilleran transposition.

At the end of the transposition, coronitic mineral growth affected the metapelites under low-*P* amphibolite facies conditions, followed by discrete $D_{T+1}$ shear zones, which deform late pegmatites (~50.5 Ma) overprinting $S_T$ in the studied transect. Relationships between $S_T$, pegmatite emplacement and $D_{T+1}$ structures are useful for timing the late extension (Fig. 13). The latter is accompanied by a further rise of the geothermal gradient compatible with the occurrence of in situ intragranular melt in metapelites and with syn-$D_{T+1}$ melt pockets (10 cm) in migmatitic rocks of the Blanket Mt. area.

The final cooling (Fig. 13) is best recorded in the GLSBZ, where Sil is microboudinaged and boudin necks are filled mainly by Chl and Wm. Rare Bt in these necks suggest a progressive transition to colder and shallower crustal levels during the development of the top-to-the-west normal shearing in the GLSBZ. The final activity of the GLSBZ was brittle, resulting in N–S trending normal and transcurrent faults (Johnston et al., 2000; Kruse and Williams, 2005) intersecting some lamprophyres, which were cooled at ca. 48 Ma and post-date $D_{T+2}$ ductile deformation (Fig. 13).

The metamorphic age data, ranging in a wide interval from ca. 1.8 Ga (e.g. Kuiper, 2003) to ca. 750 Ma (e.g. Duncan, 1984) to ca. 50 Ma (Hinchey et al., 2006), justify the occurrence of contrasting pre-$D_T$ tectonometamorphic histories. Therefore the rocks of Thor-Odin basement probably experienced structural and metamorphic events during Rodinia break up, again together with cover, during Cordilleran subduction and collision, and finally during extension-related exhumation of the dome. In this portion of Thor-Odin, the Cordilleran transposition is responsible for the near-complete annihilation of the earlier histories.

## Acknowledgements

Useful revisions by H. Daniel Gibson and Yvette D. Kuiper helped to improve the clearness of the paper. Andrew C. Parmenter and Michele Zucali are acknowledged for stimulating discussions. Andrea Risplendente, Agostino Rizzi, Douglas Hall, and Steven Cogswell provided the technical support at the SEM and EPMA. Funding by NSERC Discovery Grant (P.F.W. - University of New Brunswick) and MIUR-COFIN 2005 and PUR 2006-2008 of Università degli Studi di Milano.

## References

Adams, M.G., Lentz, D.R., Shaw, C.S.J., Williams, P.F., Archibald, D.A., Cousens, B., 2005. Eocene shoshonitic mafic dykes intruding the Monashee complex, British Columbia: a petrogenetic relationship with the Kamloops Group volcanic sequence? Canadian Journal of Earth Sciences 42, 1–15.

Armstrong, R.L., Parrish, R.R., Van Der Heyden, P., Scott, K., Runkle, D., Brown, R.L., 1991. Early Proterozoic basement exposures in the southern Canadian Cordillera: core gneiss of Frenchman Cap, unit 1 of the Grand Forks gneiss and the Vaseaux formation. Canadian Journal of Earth Sciences 28, 1169–1201.

Berthé, D., Choukroune, P., Jegouzo, P., 1979. Orthogneiss, mylonite and non-coaxial deformation of granites: the example of the South Armorican shear zone. Journal of Structural Geology 1, 31–42.

Bhattacharya, A., Mohanty, L., Maji, A., Sen, S.K., Raith, M., 1992. Non-ideal mixing in the phlogopite-annite-binary: constraints from experimental data on Mg-Fe partitioning and a formulation of the biotite-garnet geothermometer. Contributions to Mineralogy and Petrology 11, 87–93.

Bohlen, S.R., Liotta, J.J., 1986. A barometer for garnet amphibolites and garnet granulites. Journal of Petrology 27, 1025–1034.

Bohlen, S.R., Wall, V.J., Boettcher, A.L., 1983. Experimental investigations and geological applications of equilibria in the system $FeO–TiO_2–Al_2O_3–SiO_2–H_2O$. American Mineralogist 68, 1049–1058.

Brown, M., 2001. Orogeny, migmatites and leucogranite: a review. Proceedings of the Indian Academy of Science: Earth and Planetary Sciences 110, 313–336.

Brown, R.L., 1980. Frenchman Cap Dome, Shuswap Complex, British Columbia: a Progress Report. In: Current Research, Part A. Geological Survey of Canada, Ottawa, pp. 47–51.

Brown, R.L., Carr, S.D., 1990. Lithospheric thickening and orogenic collapse within the Canadian Cordillera. In: Proceedings of the Pacific Rim '90 Congress, 2. Australasian Institute of Mining and Metallurgy, Brisbane, Australia, pp. 1–10.

Brown, R.L., Carr, S.D., Johnson, B.J., Coleman, V.J., Cook, F.A., Varsek, J.L., 1992. The Monashee decollement of the southern Canadian Cordillera: a crustal-scale shear zone linking the Rocky Mountain Foreland Belt to lower crust beneath accreted terranes. In: McClay, K.R. (Ed.), Thrust Tectonics. Chapman and Hall, London, U.K, pp. 357–364.

Carr, S.D., 1991. Three crustal zones in the Thor-Odin-Pinnacles area, southern Omineca belt, British Columbia. Canadian Journal of Earth Sciences 28, 2003–2023.

Carr, S.D., 1995. The southern Omineca belt, British Columbia: new perspectives from the Lithoprobe Geoscience program. Canadian Journal of Earth Sciences 32, 1720–1739.

Cimmino, F., Messiga, B., 1979. I calcescisti del Gruppo di Voltri (Liguria occidentale): le variazioni composizionali delle miche bianche in rapporto all'evoluzione tettonico-metamorfica alpina. Ofioliti 4, 269–294.

Cloos, M., 1993. Lithospheric buoyancy and collisional orogenesis: subduction of oceanic plateaus, continental margins, island arcs, spreading ridges and seamounts. Geological Society of America Bulletin 105, 715–737.

Coleman, V.J., 1990. The Monashee Decollement at Cariboo Alp and regional kinematic indicators, southeastern British Columbia. M.Sc. thesis, Carleton University.
Crowley, J.L., 1997. U–Pb geochronologic constraints on the cover sequence of the Monashee Complex, Canadian Cordillera; Paleoproterozoic deposition on basement. Canadian Journal of Earth Sciences 34, 1008–1022.
Dalziel, I.W.D., 1997. Neoproterozoic – Paleozoic geography and tectonics: review, hypothesis, environmental speculation. Geological Society of America Bulletin 108, 16–42.
di Paola, S., Spalla, M.I., 2000. Contrasting tectonic records in pre-Alpine metabasites of the southern Alps (Lake Como, Italy). Journal of Geodynamics 30, 167–189.
Diella, V., Spalla, M.I., Tunesi, A., 1992. Contrasted thermo-mechanical evolutions in the Southalpine metamorphic basement of the Orobic Alps (Central Alps, Italy). Journal of Metamorphic Geology 10, 203–219.
Duncan, I.J., 1982. The evolution of the Thor Odin Gneiss Dome and related geochronological studies. Ph.D. thesis, University of British Columbia.
Duncan, I.J., 1984. Structural evolution of the Thor-Odin gneiss dome. Tectonophysics 101, 87–130.
Eckert, J.O., Newton, R.C., Kleppa, O.J., 1991. The $\Delta H$ of reaction and recalibration of garnet-pyroxene-plagioclase-quartz geobarometers in the CMAS system by solution calorimetry. American Mineralogist 76, 148–160.
Eisbacher, G.H., 1985. Late Proterozoic rifting, glacial sedimentation, and sedimentary cycles in the light of Windermere deposition, Western Canada. Palaeogeography, Palaeoclimatology, Palaeoecology 51, 231–254.
Ellis, D.J., Green, D.H., 1979. An experimental study on the effect of Ca upon garnet-clinopyroxene Fe–Mg exchange equilibria. Contributions to Mineralogy and Petrology 71, 13–22.
Ellis, D.J., Thompson, A.B., 1986. Subsolidus and partial melting reactions in the quartz-excess $CaO + MgO + Al_2O_3 + SiO_2 + H_2O$ system under water excess and water-deficient conditions to 10 kbar: some implications for the origin of peraluminous melts from mafic rocks. Journal of Petrology 27, 91–121.
England, P.C., Thompson, A.B., 1984. Pressure-Temperature-Time paths of regional metamorphism I. Heat transfer during the evolution of regions of thickened continental crust. Journal of Petrology 25, 894–928.
Ernst, W.G., 1979. Coexisting sodic and calcic amphiboles from high pressure metamorphic belts and the stability of barroisitic amphibole. Mineralogical Magazine 43, 269–278.
Ernst, W.G., Liou, J.G., 2008. High- and ultrahigh-pressure metamorphism: past results and future prospects. American Mineralogist 93, 1771–1786.
Ferri, F., Poli, S., Vielzeuf, D., 2009. An experimental determination of the effect of bulk composition on phase relationships in metasediments at near-solidus conditions. Journal of Petrology 50, 909–931.
Fershtater, G.B., 1990. Empirical hornblende-plagioclase geobarometer. Geokhimiya 3, 328–335.
Gabrielse, H., Monger, J.W.H., Wheeler, J.O., Yorath, C.J., 1991. Morphogeological belts, tectonics assemblages and terranes (Chapter 2), Part A. In: Gabrielse, H., Yorath, C.J. (Eds.), Geology of the Cordilleran Orogen in Canada, vol. 4. Geological Survey of Canada, pp. 15–28.
Ganguly, J., Saxena, S.K., 1984. Mixing properties of aluminosilicate garnets: constraints from natural and experimental data, and applications to geothermo-barometry. American Mineralogist 69, 88–97.
Gazzola, D., Gosso, G., Pulcrano, E., Spalla, M.I., 2000. Eo-Alpine HP metamorphism in the Permian intrusives from the steep belt of the Central Alps (Languard-Campo nappe and Tonale Series). Geodinamica Acta 13, 149–167.
Ghent, E.D., Nicholls, J., Stout, M.Z., Rottenfusser, B., 1977. Clinopyroxene amphibolite boudins from three Valley Gap, British Columbia. The Canadian Mineralogist 15, 269–282.
Gibson, H.D., Brown, R.L., Carr, S.D., 2008. Tectonic evolution of the Selkirk fan, southeastern Canadian Cordillera: a composite Middle Jurassic–Cretaceous orogenic structure. Tectonics 27, TC6007.
Graham, C.M., Powell, R., 1984. A garnet-hornblende geothermometer; calibration, testing, and application to the Pelona Schist, Southern California. Journal of Metamorphic Geology 2, 13–31.
Guidotti, C.V., Cheney, J.T., Conatore, P.D., 1975. Interrelationships between Mg/Fe and octahedral Al content in biotite. American Mineralogist 60, 849–853.
Hammarstrom, J., Zen, E.a., 1986. Aluminum in hornblende; an empirical geobarometer. American Mineralogist 71, 1297–1313.
Henry, D., Guidotti, C.V., Thomson, J., 2005. The Ti-saturation surface for low-to-medium pressure metapelitic biotites: implications for geothermometry and Ti-substitution mechanisms. American Mineralogist 90, 316–328.
Hey, M.H., 1954. A new review of the chlorites. Mineralogical Magazine 30, 277–292.
Hinchey, A.M., 2005. Thor-Odin dome: constraints on Paleocene-Eocene anatexis and deformation, leucogranite generation and the tectonic evolution of the Southern Omineca belt, Canadian Cordillera. Ph.D. thesis, Carleton University.
Hinchey, A.M., Carr, S.D., McNeill, P.D., Rayner, N., 2006. Paleocene-Eocene high-grade metamorphism, anatexis and deformation in the Thor-Odin dome, Monashee complex, southeastern British Columbia. Canadian Journal of Earth Sciences 43, 1341–1365.
Hobbs, B.E., Ord, A., Spalla, M.I., Gosso, G., Zucali, M., 2010. The interaction of deformation and metamorphic reactions. In: Spalla, M.I., Marotta, A.M., Gosso, G. (Eds.), Advances in Interpretation of Geological Processes: Refinement of Multi-scale Data and Integration in Numerical Modelling. Geological Society of London Special Publications, vol. 332, pp. 189–222.
Hodges, K.V., Crowley, P.D., 1985. Error estimation and empirical geothermobarometry for pelitic systems. American Mineralogist 70, 702–709.
Hodges, K.V., Spear, F.S., 1982. Geothermometry, geobarometry and the $Al_2SiO_5$ triple point at Mt Moosilanke, New Hampshire. American Mineralogist 69, 1118–1134.
Hoisch, T.D., 1990. Empirical calibration of six geobarometers for the mineral assemblage quartz + muscovite + biotite + plagioclase + garnet. Contributions to Mineralogy and Petrology 104, 225–234.
Holland, T.J.B., Blundy, J., 1994. Non-ideal interactions in calcic amphiboles and their bearing on amphibole-plagioclase thermometry. Contributions to Mineralogy and Petrology 116, 433–447.
Holland, T.J.B., Powell, R., 1998. An internally consistent thermodynamic data set for phases of petrological interest. Journal of Metamorphic Geology 16, 309–344.
Hollister, L.S., Grissom, G.C., Peters, E.K., Stowell, H.H., Sisson, V.B., 1987. Confirmation of the empirical correlation of Al in hornblende with pressure of solidification of calc-alkaline plutons. American Mineralogist 72, 231–239.
Holness, M.B., 2008. Decoding migmatite microstructures. In: Sawyer, E.W., Brown, M. (Eds.), Working with Migmatites, vol. 38. Mineralogical Association of Canada, pp. 57–76.
Holness, M.B., Sawyer, E.W., 2008. On the pseudomorphing of melt-filled pores during the crystallization of migmatites. Journal of Petrology 49, 1343–1363.
Jiang, D., Williams, P.F., 1998. High-strain zones: a unified model. Journal of Structural Geology 20, 1105–1120.
Johnson, C., Rutherford, M.J., 1989. Experimental calibration of the aluminium-in-hornblende geobarometer with application to Long Valley caldera (California) volcanic rocks. Geology 17, 837–841.
Johnson, S.E., Vernon, R.H., 1995. Inferring the timing of porphyroblast growth in the absence of continuity between inclusion trails and matrix foliations; can it be reliably done? Journal of Structural Geology 17, 1203–1206.
Johnston, D.H., 1998. Structural and thermal evolution of northwest Thor-Odin dome, Monashee complex, southeastern British Columbia. Ph.D. thesis, University of New Brunswick.
Johnston, D.H., Williams, P.F., Brown, R.L., Crowley, J.L., Carr, S.D., 2000. Northeastward extrusion and extensional exhumation of crystalline rocks of the Monashee Complex, southeastern Canadian Cordillera. Journal of Structural Geology 22, 603–625.
Journeay, J.M., 1986. Stratigraphy, internal strain and thermo-tectonic evolution of northern Frenchman Cap dome: an exhumed duplex structure, Omineca hinterland, S.E. Canadian Cordillera. Ph.D. thesis, Queens University.
Journeay, J.M., Brown, R.L., 1986. Major Tectonic Boundaries of the Omineca Belt in Southern British Columbia: a Progress Report. In: Geological Survey Paper Canada 86-1A, pp. 81–88.
Kohn, M.J., Spear, F.S., 1990. Two new geobarometers for garnet amphibolites, with applications to southeastern Vermont. American Mineralogist 75, 89–96.
Koziol, A.M., 1989. Recalibration of the garnet-plagioclase-$Al_2SiO_5$-quartz (GASP) geobarometer and application to natural parageneses. EOS Transactions of the American Geophysical Union 70, 493.
Kretz, R., 1983. Symbols for rock-forming minerals. American Mineralogist 68, 277–279.
Kruse, S., 2007. Structural evolution of the northern Thor-Odin culmination, Monashee Complex, southern Canadian Cordillera. Ph.D. thesis, University of New Brunswick.
Kruse, S., McNeill, P.D., Williams, P.F., 2004. Geological map of the Thor-Odin dome, southern Monashee complex, BC. http://www.unb.ca/fredericton/science/geology/monashee.
Kruse, S., Williams, P.F., 2005. Brittle faulting in the Thor-Odin culmination, Monashee complex, southern Canadian Cordillera: constraints on geometry and kinematics. Canadian Journal of Earth Sciences 42, 2141–2160.
Kruse, S., Williams, P.F., 2007. The Monashee reflector: re-examining a Lithoprobe crustal-scale reflector in the southern Canadian Cordillera. Geosphere 3. doi:10.1130/GES00049.1.
Kuiper, Y.D., 2003. Isotopic constraints on timing of deformation and metamorphism in Thor-Odin, Monashee complex, southeastern BC. Ph.D thesis, University of New Brunswick.
Kuiper, Y.D., Williams, P.F., Kruse, S., 2006. Possibility of channel flow in the Southern Canadian Cordillera: a new approach to explain existing data. In: Law, R.D., Searle, M.P., Godin, L. (Eds.), Channel Flow, Ductile Extrusion and Exhumation in Continental Collision Zones, vol. 268. The Geological Society of London, London, pp. 589–611.
Laird, J., Albee, A.L., 1981. Pressure, temperature and time indicators in mafic schists: their application to reconstructing the polymetamorphic history of Vermont. American Journal of Science 281, 127–175.
Lane, L.S., Ghent, E.D., Stout, M.Z., Brown, R.L., 1989. P-T history and kinematics of the Monashee décollement near Revelstoke, British Columbia. Canadian Journal of Earth Sciences 26, 231–243.
Lardeaux, J.M., Gosso, G., Kienast, J.R., Lombardo, B., 1983. Chemical variations in phengitic micas of successive foliations within the Eclogitic Micaschists complex, Sesia-Lanzo zone (Italy, Western Alps). Bulletin de Minéralogie 106, 673–689.
Le Breton, N., Thompson, A.B., 1988. Fluid-absent (dehydration) melting of biotite in metapelites in the early stages of crustal anatexis. Contributions to Mineralogy and Petrology 99, 226–237.
Leake, B.E., Woolley, A.R., Arps, C.E.S., Birch, W.D., Gilbert, M.C., Grice, J.D., Hawthorne, F.C., Kato, A., Kisch, H.J., Krivovichev, V.G., Linthout, K., Laird, J., Mandarino, J.A., Maresch, W.V., Nickel, E.H., Rock, N.M.S., Schumacher, J.C., Smith, D.C., Stephenson, N.C.N., Ungaretti, L., Whittaker, E.J.W., Guo, Y., 1997.

Nomenclature of amphiboles; report of the subcommittee on amphiboles of the International Mineralogical Association, commission on new minerals and mineral names. American Mineralogist 82, 1019–1037.
Léger, A., Ferry, J.M., 1991. Highly aluminous hornblende from low-pressure metacarbonates and a preliminary thermodynamic model for the Al content of calcic amphibole. American Mineralogist 76, 1002–1017.
Li, Z.X., Bogdanova, S.V., Collins, A.S., Davidson, A., De Waele, B., Ernst, R.E., Fitzsimons, I.C.W., Fuck, R.A., Gladkochub, D.P., Jacobs, J., Karlstrom, K.E., Lul, S., Natapovm, L.M., Pease, V., Pisarevsky, S.A., Thrane, K., Vernikovsky, V., 2008. Assembly, configuration, and break-up history of Rodinia: a synthesis. Precambrian Research 160, 179–210.
Liou, J.G., Bohlen, S.R., Ernst, W.G., 1996. Stability of hydrous phases in subducting oceanic crust. Earth and Planetary Science Letters 143, 161–171.
Liou, J.G., Kuniyoshi, S., Ito, K., 1974. Experimental studies of the phase relations between greenschist and amphibolites in a basaltic system. American Journal of Science 274, 613–632.
Lister, G.S., Williams, P.F., 1983. The partitioning of deformation in flowing rock masses. Tectonophysics 92, 1–33.
Lorencak, M., Seward, D., Vanderhaeghe, O., Teyssier, C., Burg, J.P., 2001. Low-temperature cooling history of the Shuswap metamorphic core complex, British Columbia: constraints from apatite and zircon fission-track ages. Canadian Journal of Earth Sciences 38, 1615–1625.
Massonne, H.J., Schreyer, W., 1987. Phengite geobarometry based on the limiting assemblage with K-feldspar, phlogopite and quartz. Contributions to Mineralogy and Petrology 96, 212–224.
McNicoll, V.J., Brown, R.L., 1995. The Monashee decollement at Cariboo Alp, southern flank of the Monashee complex, southern British Columbia, Canada. Journal of Structural Geology 17, 17–30.
Moecher, D.P., Essene, E.J., Anovitz, L.M., 1988. Calculation and application of clinopyroxene-garnet-plagioclase-quartz geobarometers. Contributions to Mineralogy and Petrology 100, 92–106.
Monger, J.W.H., Price, R.A., Tempelman-Kluit, D.J., 1982. Tectonic accretion and the origin of the two major metamorphic and plutonic welts in the Canadian Cordillera. Geology 10, 70–75.
Moody, J.B., Meyer, D., Jenkins, J.E., 1983. Experimental characterization of the greenschist/amphibolite boundary in mafic system. American Journal of Science 283, 48–92.
Morimoto, N., 1988. Nomenclature of pyroxenes. Mineralogical Magazine 52, 535–550.
Newton, R.C., Haselton, H.T., 1981. Thermodynamics of the garnet-plagioclase-$Al_2SiO_5$-quartz geobarometer. In: Newton, R.C., Navrotsky, A., Wood, B.J. (Eds.), Thermodynamics of Melts and Minerals. Springer-Verlag, New York, pp. 131–147.
Norlander, B.H., Whitney, D.L., Teyssier, C., Vanderhaeghe, O., 2002. Partial melting and decompression of the Thor-Odin dome, Shuswap metamorphic complex, Canadian Cordillera. Lithos 61, 103–125.
Nyman, M.W., Pattison, D.R.M., Ghent, E.D., 1995. Melt extraction during formation of K-Feldspar + Sillimanite migmatites, west of Revelstoke, British Columbia. Journal of Petrology 36, 351–372.
Okulitch, A.V., 1984. The role of the Shuswap metamorphic complex in Cordilleran tectonism: a review. Canadian Journal of Earth Sciences 21, 1171–1193.
Otten, M.T., 1984. The origin of brown hornblende in the Artfjaellet gabbro and dolerites. Contributions to Mineralogy and Petrology 86, 189–199.
Parkinson, D.L., 1991. Age and isotopic character of Early Proterozoic basement gneisses in the southern Monashee Complex, southeastern British Columbia. Canadian Journal of Earth Sciences 28, 1159–1168.
Parkinson, D.L., 1992. Age and tectonic evolution of the southern Monashee complex, southeastern British Columbia: a window into the deep crust. Ph.D. thesis, University of Santa Barbara.
Parrish, R.R., Carr, S.D., Parkinson, D.L., 1988. Eocene extensional tectonics and geochronology of the southern Omineca belt, British Columbia and Washington. Tectonics 7, 181–212.
Passchier, C.W., Trouw, R.A.J., 1996. Microtectonics. Springer, Berlin, Heidelberg, New York.
Perchuk, L.L., Aranovich, L.Y., Podlesskii, K.K., Lavrent'eva, I.V., Gerasimov, V.Y., Fed'Kin, V.V., Kitsul, V.I., Karasakov, L.P., Berdnikov, N.V., 1985. Precambrian granulites of the Aldan shield eastern Siberia, USSR. Journal of Metamorphic Geology 3, 265–310.
Perchuk, L.L., Lavrent'eva, I.V., 1983. Experimental investigation of exchange equilibria in the system cordierite-garnet-biotite. In: Saxena, S.K. (Ed.), Kinetics and Equilibrium in Mineral Reactions. Springer-Verlag, New York, pp. 199–239.
Plyusnina, L.P., 1982. Geothermometry and geobarometry of plagioclase-hornblende bearing assemblages. Contributions to Mineralogy and Petrology 80, 140–146.
Poli, S., Schmidt, M.W., 1995. $H_2O$ transport and release in subduction zones: experimental constraints on basaltic and andesitic system. Journal of Geophysical Research 100, 22299–22314.
Powell, R., 1985. Regression diagnostics and robust regression in geothermometer/geobarometer calibration: the garnet-clinopyroxene geothermometer revised. Journal of Metamorphic Geology 3, 231–243.
Read, P.B., Brown, R.L., 1981. Columbia River fault zone; southeastern margin of the Shuswap and Monashee complexes, southern British Columbia. Canadian Journal of Earth Sciences 18, 1127–1145.
Reesor, J.E., Moore Jr., J.M., 1971. Petrology and Structure of Thor-Odin Gneiss Dome, Shuswap Metamorphic Complex, British Columbia. In: Geological Survey of Canada Paper, vol. 195, 149 pp.
Rosenberg, C.L., Riller, U., 2000. Partial-melt topology in statically and dynamically recrystallized granite. Geology 28, 7–10.
Ross, G.M., Parrish, R.R., 1991. Detrital zircon geochronology of metasedimentary rocks in the southern Omineca Belt, Canadian Cordillera. Canadian Journal of Earth Sciences 28, 1254–1270.
Rushmer, T., 1993. Experimental high-pressure granulites: some application to natural mafic xenolith suites and Archean granulite terrane. Geology 21, 411–414.
Schmidt, M.W., 1992. Amphibole composition in tonalite as a function of pressure: an experimental calibration of the Al-in-hornblende barometer. Contributions to Mineralogy and Petrology 110, 304–310.
Shields, C., Kuiper, Y.D., 2008. New detrital and metamorphic zircon ages from cover rocks of the Monashee complex, Southeastern Canadian Cordillera. In: GSA, Northeastern Section 43rd Annual Meeting 40, Buffalo, NY, USA, p. 19.
Spalla, M.I., 1993. Microstructural control on the P-T path construction in the metapelites from the Austroalpine crust (Texel Gruppe, Eastern Alps). Schweizerische Mineralogische und Petrographische Mitteilungen 73, 259–275.
Spalla, M.I., Gosso, G., Marotta, A.M., Zucali, M., Salvi, F., 2010. Analysis of natural tectonic systems coupled with numerical modelling in the polycyclic continental lithosphere of the Alps. International Geology Review 52, 1268–1302.
Spalla, M.I., Marotta, A.M., 2007. P–T evolutions vs. numerical modeling: a key to unravel the Paleozoic to Early-Mesozoic tectonic evolution of the Alpine area. Periodico di Mineralogia 76, 267–308.
Spalla, M.I., Siletto, G.B., di Paola, S., Gosso, G., 2000. The role of structural and metamorphic memory in the distinction of tectono-metamorphic units: the basement of the Como lake in the Southern Alps. Journal of Geodynamics 30, 191–204.
Spark, R.N., 2001. Crustal thickening and tectonic denudation within the Thor-Odin culmination, Monashee complex, southern Canadian Cordillera. Ph.D. thesis, University of New Brunswick.
Spear, F.S., 1993. Metamorphic Phase Equilibria and Pressure-Temperature-Time Paths. BookCrafters, Inc., Chelsea, Michigan.
Spear, F.S., Cheney, J.T., 1989. A petrogenetic grid for pelitic schist in the system $SiO_2$–$Al_2O_3$–FeO–MgO–$K_2O$–$H_2O$. Contributions to Mineralogy and Petrology 101, 149–164.
Stöckhert, B., Gerya, T.V., 2005. Pre-collisional high pressure metamorphism and nappe tectonics at active continental margins: a numerical simulation. Terra Nova 17, 102–110.
Thompson, A.B., 1981. The pressure–temperature (P, T) plane viewed by geophysicists and petrologists. Terra Cognita 1, 11–20.
van Rooyen, D., Carr, S.D., Murphy, D., 2010. LA-ICP-MS detrital zircon results from quartzites in the Thor-Odin – pinnacles area: constraints on age and provenance, and implications for models of allochthonous vs autochthonous deposition. In: Cordilleran Tectonics Workshop 2010, Ottawa, ON, Canada, pp. 36–39.
Vanderhaeghe, O., Teyssier, C., McDougall, I., Dunlap, W., 2003. Cooling and exhumation of the Shuswap metamorphic core complex constrained by $^{40}Ar/^{39}Ar$ thermochronology. Geological Society of America Bulletin 115, 200–216.
Vanderhaeghe, O., Teyssier, C., Wysoczansky, R., 1999. Structural and geochronological constraints on the role of partial melting during the formation of the Shuswap metamorphic core complex at the latitude of the Thor-Odin dome, British Columbia. Canadian Journal of Earth Sciences 36, 917–943.
Vernon, R.H., 1989. Evidence of syndeformational contact metamorphism from porphyroblast-matrix microstructural relationship. Tectonophysics 158, 113–126.
Wanless, R.K., Reesor, J.E., 1975. Precambrian zircon age of orthogneiss in the Shuswap metamorphic complex, British Columbia. Canadian Journal of Earth Sciences 12, 326–332.
Whitney, D.L., Evans, B.D.W., 2010. Abbreviations for names of rock-forming minerals. American Mineralogist 95, 185–187.
Williams, P.F., 1985. Multiply deformed terrains – problems of correlation. Journal of Structural Geology 7, 269–280.
Williams, P.F., Jiang, D., 2005. An investigation of lower crustal deformation: evidence for channel flow and its implications for tectonics and structural studies. Journal of Structural Geology 27, 1486–1504.
Wu, C.M., Zhang, J., Ren, L.D., 2004. Empirical Garnet–Biotite–Plagioclase–Quartz (GBPQ) geobarometry in medium- to high-grade metapelites. Journal of Petrology 45, 1907–1921.